

R-0 1/2  
NASA CR-135046  
R77AEG177

The NASA logo, featuring the word "NASA" in a bold, sans-serif font, with a stylized orbital path or wing design above it.

QUIET CLEAN SHORT-HAUL EXPERIMENTAL ENGINE  
(QCSEE)  
UNDER-THE-WING ENGINE COMPOSITE FAN BLADE  
FINAL DESIGN TEST REPORT

February 1977

by

Advanced Engineering & Technology Programs Department  
General Electric Company

(NASA-CR-135046) QUIET CLEAN SHORT-HAUL  
EXPERIMENTAL ENGINE (QCSEE) UNDER-THE-WING  
ENGINE COMPOSITE FAN BLADE DESIGN REPORT  
Final Report (General Electric Co.) 61 p  
HC A04/MP A01


7 N80-15108

CSCL 21F 63/07 Unclas  
33490

Prepared for

**National Aeronautics and Space Administration**

NASA Lewis Research Center  
Contract NAS3-18021

A handwritten signature or mark, possibly "J. G. L. 1/2/77", located at the bottom right of the page.

1. Report No. NASA CR-135046	2. Government Accession No.	3. Recipient's Catalog No.	
4. Title and Subtitle  QUIET CLEAN SHORT-HAUL EXPERIMENTAL ENGINE (QCSEE) UTW Engine Composite Fan Blade Final Design Test Report		5. Report Date February 1977	
		6. Performing Organization Code	
7. Author(s) R. Ravenhall, C.T. Saleme and R.G. Stabrylla		8. Performing Organization Report No. R77AEG177	
9. Performing Organization Name and Address General Electric Company Aircraft Engine Group Cincinnati, Ohio 45215		10. Work Unit No.	
		11. Contract or Grant No. NAS3-18021	
12. Sponsoring Agency Name and Address  National Aeronautics and Space Administration Washington, D.C. 20546		13. Type of Report and Period Covered Contractor Report	
		14. Sponsoring Agency Code	
15. Supplementary Notes Test Report, Project Manager, C.C. Ciepluch, QCSEE Project Office Technical Adviser, Morgan Hanson NASA Lewis Research Center, Cleveland, Ohio 44135			
16. Abstract  This report presents the results of tests conducted on final QCSEE design polymeric - composite fan blades for the Under-the-Wing (UTW) engine.  During this phase of the program a total of 38 QCSEE UTW composite fan blades were manufactured for various component tests, process and tooling, checkout, and use in the QCSEE UTW engine. The component tests included frequency characterization, strain distribution, bench fatigue, platform static load, whirligig high cycle fatigue, whirligig low cycle fatigue, whirligig strain distribution and whirligig overspeed. All tests were successfully completed. All blades planned for use in the engine were subjected to and passed a whirligig proof spin test.			
17. Key Words (Suggested by Author(s)) Composite Blades Fan Blades Aerodynamics Aircraft Propulsion and Power Variable Pitch Fan			
19. Security Classif. (of this report) Unclassified	20. Security Classif. (of this page) Unclassified	21. NO. OF PAGES 55	---

### FOREWORD

This report was prepared by the Aircraft Engine Group of the General Electric Company, under contract NAS3-18021, for the NASA Lewis Research Center, Cleveland, Ohio. Mr. Morgan Hanson was the NASA UTW Composite Blade Project Manager.

This report covers the testing conducted on the final design Under-The-Wing (UTW) composite fan blade.

PRECEDING PAGE BLANK NOT FILMED

## TABLE OF CONTENTS

<u>Section</u>	<u>Page</u>
1.0 SUMMARY	1
2.0 INTRODUCTION	2
3.0 DESIGN CONFIGURATION	3
3.1 Blade Configuration	3
3.2 Blade Layup/Material Selection	3
4.0 FABRICATION	15
4.1 Raw Material Control	15
4.2 Blade Molding	16
4.3 Molding Inspection and Finishing Operations	16
4.4 Nondestructive Evaluation	18
5.0 UTW COMPOSITE BLADE TESTING	23
5.1 Blade Frequency Characteristics	23
5.2 Platform Bench Test	23
5.3 Bench Strain Distribution	29
5.4 Bench Fatigue Tests	29
6.0 WHIRLIGIG TESTING	38
6.1 Whirligig Strain Distribution	38
6.2 Cyclic Testing	48
6.3 Overspeed Proof Testing	48
6.4 High Cycle Fatigue Testing	48
6.5 Blade Proof Testing	53
7.0 CONCLUSIONS	54
8.0 REFERENCES	55

## LIST OF ILLUSTRATIONS

<u>Figure</u>		<u>Page</u>
1.	QCSEE UTW Composite Blade with Platform.	4
2.	Molded QCSEE UTW Blade.	5
3.	Blade Airfoil Sections.	6
4.	Composite Blade with Leading Edge Protection.	7
5.	Platform Construction.	8
6.	General Arrangement of Plys, QCSEE UTW Blade.	10
7.	Ply Layup and Material Arrangement.	13
8.	Molding Procedure for PR288/Type AS Blade.	17
9.	Test Technique for Ultrasonic C-Scan.	19
10.	Laser Holographic Facility.	21
11.	Holograph NDT of QCSEE Blade.	22
12.	Blade Platform Load Test Setup.	27
13.	Platform Load Test Deflections.	28
14.	Bench Test Blade Instrumentation, Blade S/N Q11.	30
15.	Bench Test Blade Instrumentation, Blade S/N Q9.	33
16.	Posttest Evaluation, Blade S/N Q9.	36
17.	Posttest Evaluation, Blade S/N Q11.	37
18.	Whirligig Test Blade Instrumentation, Blade S/N Q7.	39
19.	Whirligig Facility Test Cell.	40
20.	Assembled Blade, Trunnion and Disk.	41
21.	Whirligig Test Instrumentation Lead-Out.	42
22.	Predicted Campbell Diagram, QCSEE UTW Fan Blade.	43

LIST OF ILLUSTRATIONS (Concluded)

<u>Figure</u>		<u>Page</u>
23.	Experimentally Determined Campbell Diagram.	46
24.	Steady-State Stress Distribution.	47
25.	Blade Q6 Outsert After Testing.	49
26.	Posttest Evaluation, Blade S/N Q7.	51
27.	Stress Range Diagram.	52

## LIST OF TABLES

<u>Table</u>		<u>Page</u>
I	QCEE UTW Composite Blade Design Parameters.	9
II	Composite Blade Test Summary.	24
III	Blade Frequency Inspection Summary.	25
IV	Bench Fatigue Relative Strain Distribution - Blade S/N Q11.	31
V	Bench First Flexural High Cycle Fatigue Test Summary, Blade S/N Q9.	34
VI	Whirligig Strain Distribution - Relative Dynamic Strain Summary.	44
VII	Steady-State Stress Distribution Summary.	45
VIII	Whirligig First Flexural High Cycle Fatigue Test Summary, Blade S/N Q7.	50
IX	Blades Subjected to Whirligig Proof Test.	53

## 1.0 SUMMARY

This report presents the results of tests conducted on final design QCSEE composite fan blades. The test program was conducted to evaluate the blade's structural and dynamic capabilities and to evaluate the relationship of the blades capabilities with those anticipated from analysis and testing conducted on preliminary design blades. The purpose of the testing was also to make sure that the blade design satisfies static engine operating conditions and to obtain data to be used in setting engine operating limits.

The final blade design incorporates the results of testing and analysis conducted on preliminary design blades in an earlier phase of the program (see References 1 & 2). The final blades also incorporate features making the blades operable with a variable pitch mechanism which allows the blades to rotate through both stall and flat pitch conditions.

During this final phase of the program, a total of 38 QCSEE UTW composite fan blades were manufactured for component testing, processing and tooling checkout and engine use. Four of these blades plus one of the preliminary blades with a platform attached were used for component testing.

The component testing included platform bench and whirligig testing plus blade frequency characteristics, strain distribution, bench fatigue, whirligig high cycle fatigue, whirligig low cycle fatigue, whirligig strain distribution and whirligig overspeed.

The test results show that the blades have satisfactory margins of safety for the structural and aeromechanical requirements of the engine. The testing also provided the necessary data to indicate safe engine operation.



## 2.0 INTRODUCTION

The Quiet Clean Short-Haul Experimental Engine Program provides for the design, fabrication, and testing of experimental, high-bypass, geared turbofan engines and propulsion systems for short-haul passenger aircraft. The overall objective of the program is to develop the propulsion technology required for future externally blown flap types of aircraft with engines located both under-the-wing and over-the-wing.

This report presents the results of tests conducted on final design QCSEE composite fan blades to evaluate the blades structural and dynamic capabilities and establish the blades suitability for engine operation.

Testing conducted on preliminary design blades was reported in the QCSEE UTW Engine Composite Fan Blade Preliminary Design Test Report, NASA CR-134846 (Reference 2). Data from this earlier effort is applicable to this study.

### 3.0 DESIGN CONFIGURATION

#### 3.1 BLADE CONFIGURATION

The finished QCSEE Composite fan blade is shown in Figure 1. It consists of a molded composite blade, a molded composite platform and a metal outsert on the dovetail. The molded blade configuration is shown in Figure 2 and is made up of a solid composite airfoil and a straight bell-shaped composite dovetail. The dovetail is undercut at the leading and trailing edges to permit better transitioning of the cambered airfoil section into the straight dovetail. The airfoil definition is described by 15 radially spaced airfoil cross sections which are stacked on a common axis as shown in Figure 3. The dovetail axial centerline is offset from the stacking axis by 0.254 cm (0.1 in.) to provide a smooth airfoil-to-dovetail transition. The molded blade is provided with a reduced leading edge thickness to allow a final coating of wire mesh/nickel plate for leading edge protection. The blade leading edge protection is shown on the finished blade drawing (see Figure 4). The platform construction is shown in Figure 5.

A summary of the aero blade parameters is presented in Table I. The low root solidity of 0.98 is required for reverse pitch operation. Except for the large tip chord (high blade flare), the blade length, thickness, and twist dimensions are similar to previous composite blades which have undergone extensive development and proof testing.

#### 3.2 BLADE LAYUP/MATERIAL SELECTION

The material selection and ply arrangement for the UTW hybrid composite blade is based on previous development efforts conducted by General Electric and sponsored by NASA under Contract NAS3-16777. This work led to the selection of a combination of fibers in a single blade to provide the proper frequency response characteristics to satisfy STOL engine conditions. Figure 6 shows the general arrangement of the plies in the QCSEE UTW composite blade. The surface plies in the lower region of the blade contain S-glass fibers to increase blade flexibility. These plies, being near the surface and having relatively low bending stiffness and high tensile strength, provide higher strain-to-failure characteristics. Torsional stiffening plies in the airfoil region of the blade are oriented at  $\pm 45^\circ$  to provide the shear modulus required for a high first torsion frequency. These plies contain boron towards the outer surfaces of the blade and graphite (Hercules AS) in the inner regions.

Plies of Kevlar-49 are interspersed throughout the blade with the majority of them being in the spanwise (radial) direction of the blade. Several of the Kevlar-49 plies in the tip region of the blade are oriented at  $90^\circ$  to the spanwise axis to provide chordwise strength and stiffness to the blade.

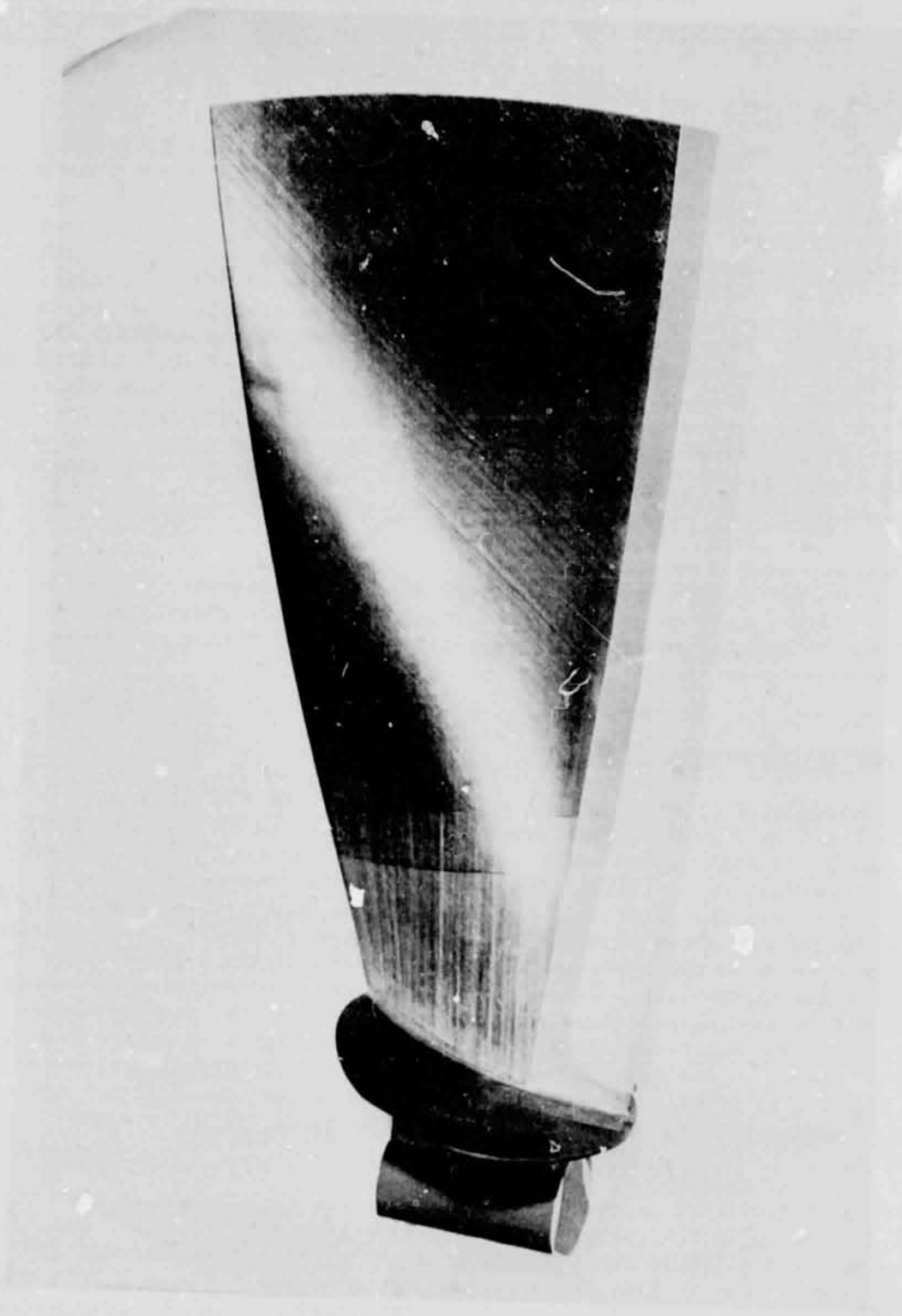


Figure 1. QCSEE UTW Composite Blade with Platform (C76011062).

ORIGINAL PAGE IS  
OF POOR QUALITY

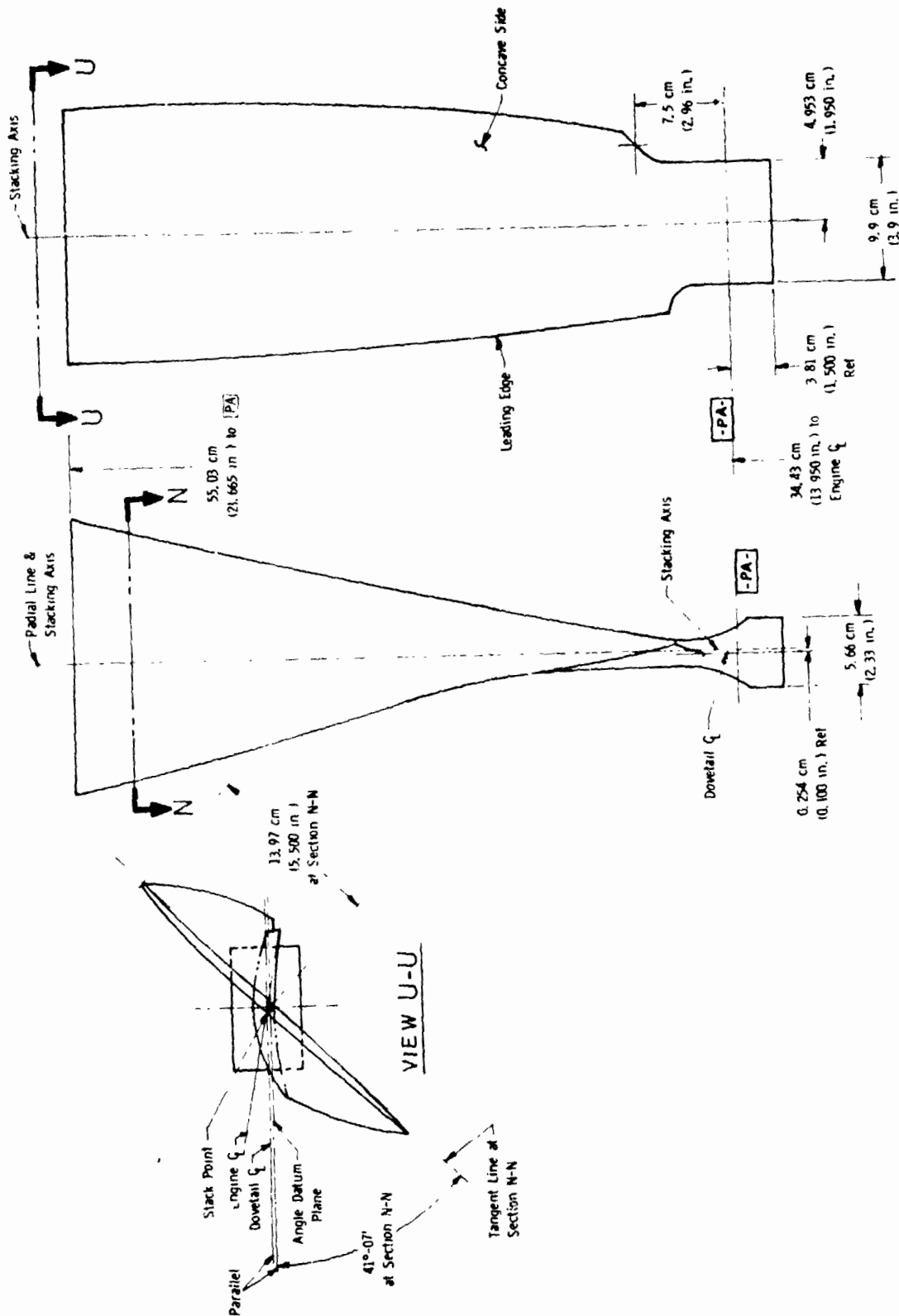
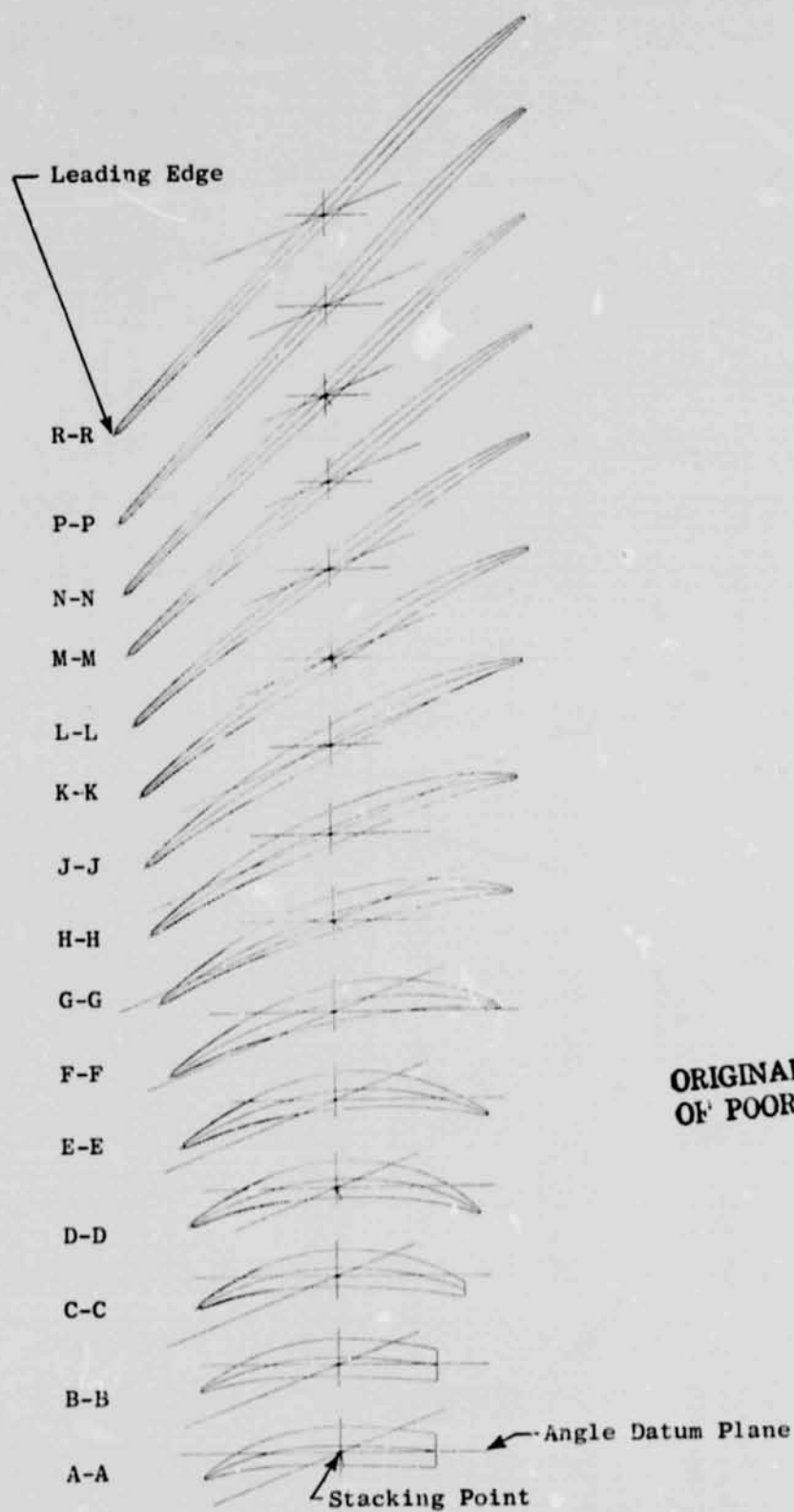


Figure 2. M. SEE UTW Blade.



ORIGINAL PAGE IS  
OF POOR QUALITY

Figure 3. Blade Airfoil Sections.

ORIGINAL PAGE IS  
OF POOR QUALITY

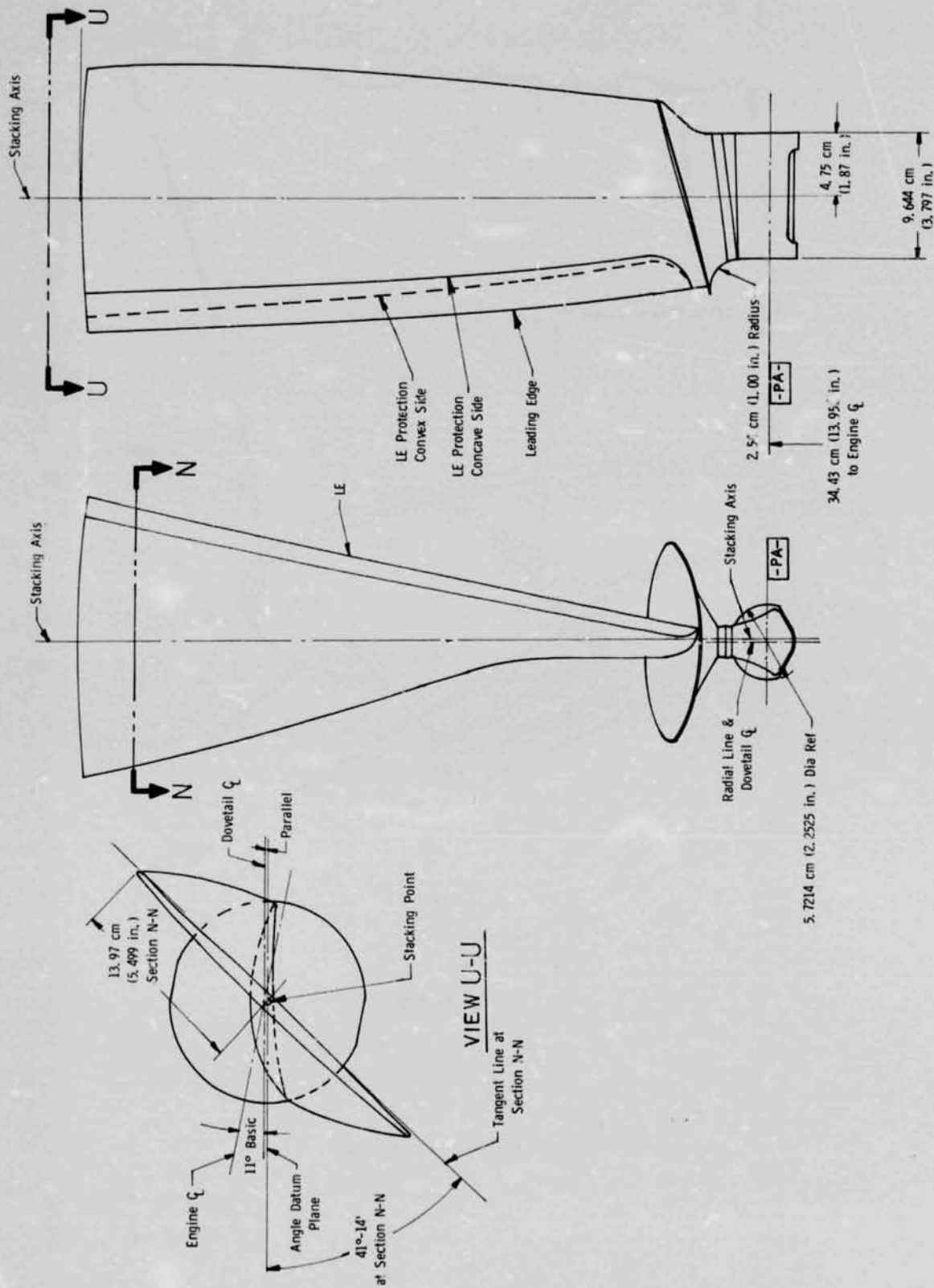


Figure 4. Composite Blade with Leading Edge Protection.

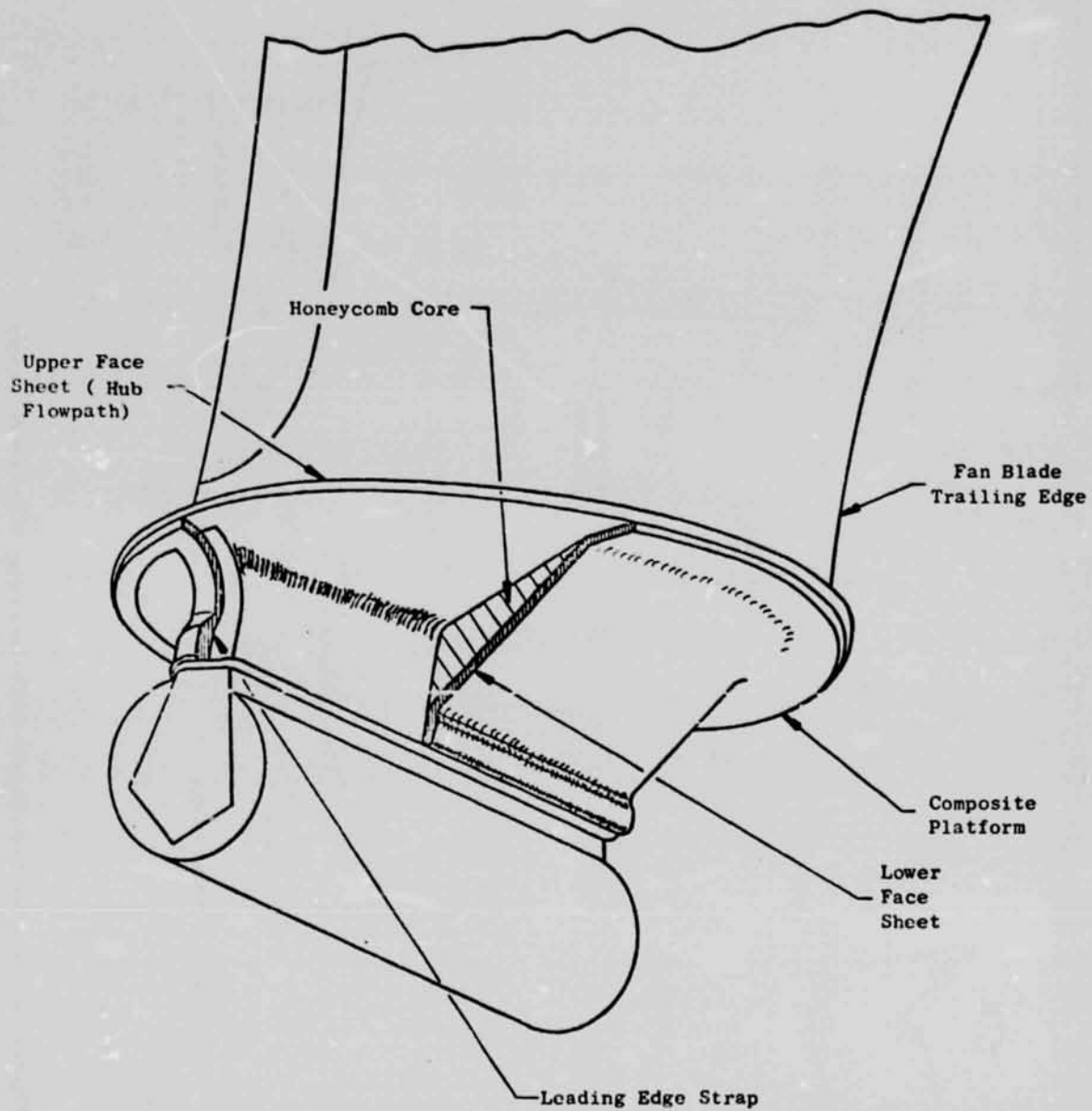


Figure 5. Platform Construction.

ORIGINAL PAGE IS  
OF POOR QUALITY

Table 1. QCSEE - UTW Composite Blade Design Parameters.

Aero Definition

Tip Speed	306 m/sec (1005 ft/sec)
Tip Diameter	180 cm (71 in.)
Radius Ratio	0.44
Number of Blades	18
Bypass Pressure Ratio	1.27 Takeoff
Aspect Ratio	2.11
Tip Chord	30.3 cm (11.91 in.)
Root Chord	14.8 cm (5.82 in.)
$T_M$ Root	1.93 cm (0.76 in.)
$T_M$ Tip	0.91 cm (0.36 in.)
Root Camber	66.2°
Total Twist	45°
Solidity	
Tip	0.95
Root	0.98
Angle Change from Forward to Reverse	
Through Flat Pitch	75°
Through Stall	100°



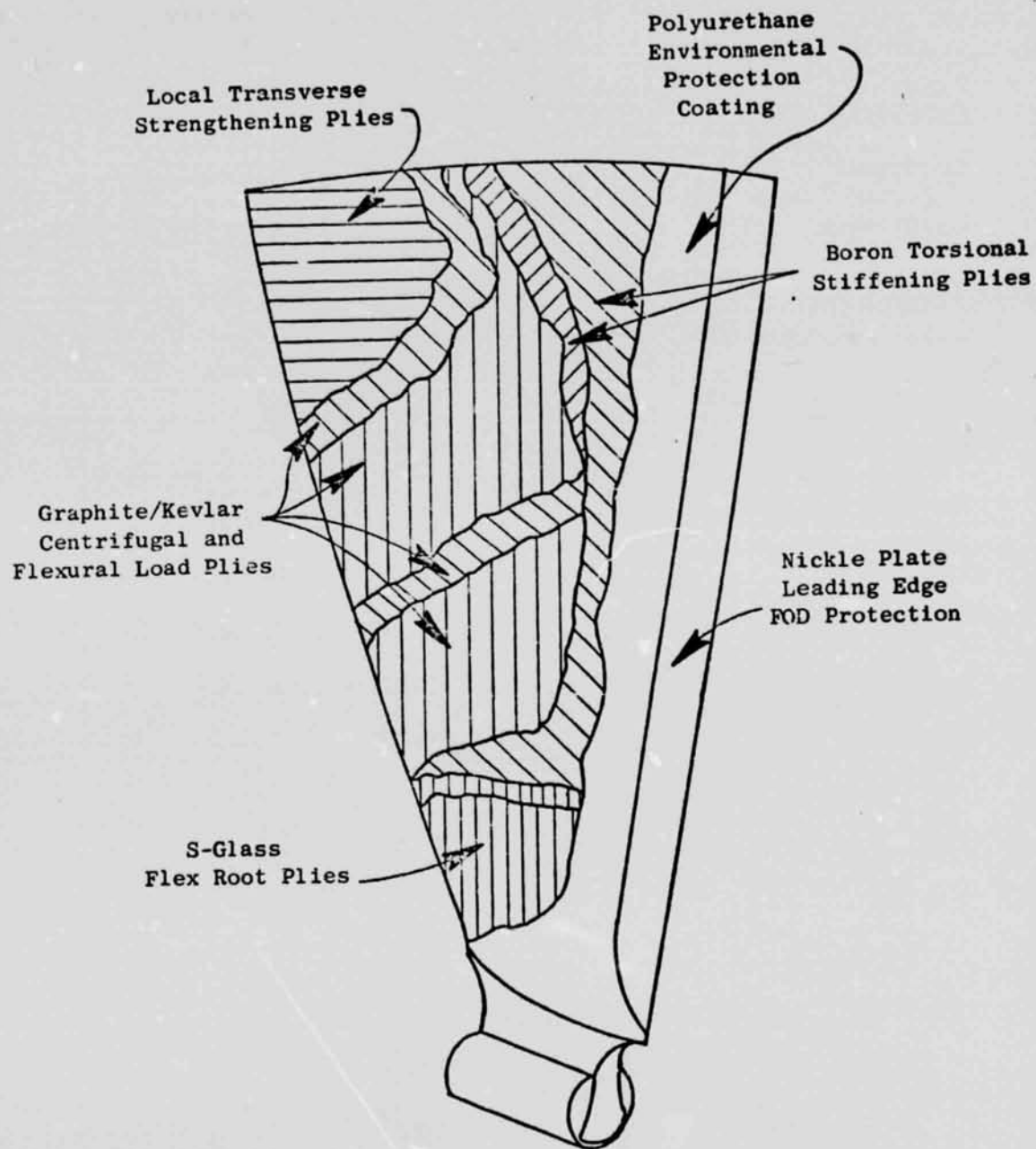


Figure 6. General Arrangement of Plys, QCSEE-UTW Blade.

The resin system used in this program is a product of the 3M Company and is designated as PR 288. This is a resin system that has proven satisfactory for the needs of advanced composite blading. Some of its unique characteristics in the prepreg form are:

- has consistent processing characteristics
- can be prepregged with many different fibers including hybrids
- uniform prepreg thickness and resin content

The general ply shapes, layup arrangement, fiber orientations and material in each ply of the blade is shown in Figure 7. This final design blade has essentially the same configuration and ply layup arrangement as tested with the preliminary blades. The material systems were changed to reflect the results of analyses and testing conducted on the preliminary blades. The preliminary blade materials are outlined in the QCSEE UTW Engine Composite Fan Blade Preliminary Test Report NASA CR-134846 (Reference 2).

FOLDOUT FRAME

PRECEDING PAGE BLANK NOT

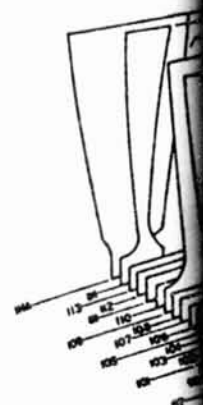
ORIGINAL PAGE IS  
OF POOR QUALITY

PLY NO.	PLY ORIENT ANGLE	MATERIAL
AIRFOIL	INSERT	
1	0°	GR
2	0°	GR
3	0°	GR
4	0°	GR
5	0°	GR
6	0°	GR
7	0°	GR
8	0°	GR
9	0°	GR
10	0°	GR
11	0°	GR
12	0°	GR
13	0°	GR
14	0°	GR
15	0°	GR
16	0°	GR
17	0°	GR
18	0°	GR
19	0°	GR
20	0°	GR
21	0°	GR
22	0°	GR
23	0°	GR
24	0°	GR
25	0°	GR
26	0°	GR
27	0°	GR
28	0°	GR
29	0°	GR
30	0°	GR
31	0°	GR
32	0°	GR
33	0°	GR
34	0°	GR
35	0°	GR
36	0°	GR
37	0°	GR
38	0°	GR
39	0°	GR
40	0°	GR
41	0°	GR
42	0°	GR
43	0°	GR
44	0°	GR
45	0°	GR
46	0°	GR
47	0°	GR
48	0°	GR
49	0°	GR
50	0°	GR
51	0°	GR
52	0°	GR
53	0°	GR
54	0°	GR
55	0°	GR
56	0°	GR
57	0°	GR
58	0°	GR
59	0°	GR
60	0°	GR
61	0°	GR
62	0°	GR
63	0°	GR
64	0°	GR
65	0°	GR
66	0°	GR
67	0°	GR
68	0°	GR
69	0°	GR
70	0°	GR
71	0°	GR
72	0°	GR
73	0°	GR
74	0°	GR
75	0°	GR
76	0°	GR
77	0°	GR
78	0°	GR
79	0°	GR
80	0°	GR
81	0°	GR
82	0°	GR
83	0°	GR
84	0°	GR
85	0°	GR
86	0°	GR
87	0°	GR
88	0°	GR
89	0°	GR
90	0°	GR
91	0°	GR
92	0°	GR
93	0°	GR
94	0°	GR
95	0°	GR
96	0°	GR
97	0°	GR
98	0°	GR
99	0°	GR
100	0°	GR

\* CONTINUATION OF PLYS IN TOP SECTION

PLY NO.	PLY ORIENT ANGLE	MATERIAL
AIRFOIL	INSERT	
99	0°	GR
100	0°	GR
101	0°	GR
102	0°	GR
103	0°	GR
104	0°	GR
105	0°	GR
106	0°	GR
107	0°	GR
108	0°	GR
109	0°	GR
110	0°	GR
111	0°	GR
112	0°	GR
113	0°	GR
114	0°	GR
115	0°	GR
116	0°	GR
117	0°	GR
118	0°	GR
119	0°	GR
120	0°	GR
121	0°	GR
122	0°	GR
123	0°	GR
124	0°	GR
125	0°	GR
126	0°	GR
127	0°	GR
128	0°	GR
129	0°	GR
130	0°	GR
131	0°	GR
132	0°	GR
133	0°	GR
134	0°	GR
135	0°	GR
136	0°	GR
137	0°	GR
138	0°	GR
139	0°	GR
140	0°	GR
141	0°	GR
142	0°	GR
143	0°	GR
144	0°	GR
145	0°	GR
146	0°	GR
147	0°	GR
148	0°	GR
149	0°	GR
150	0°	GR
151	0°	GR
152	0°	GR
153	0°	GR
154	0°	GR
155	0°	GR
156	0°	GR
157	0°	GR
158	0°	GR
159	0°	GR
160	0°	GR
161	0°	GR
162	0°	GR
163	0°	GR
164	0°	GR
165	0°	GR
166	0°	GR
167	0°	GR
168	0°	GR
169	0°	GR
170	0°	GR
171	0°	GR
172	0°	GR
173	0°	GR
174	0°	GR
175	0°	GR
176	0°	GR
177	0°	GR
178	0°	GR
179	0°	GR
180	0°	GR
181	0°	GR
182	0°	GR
183	0°	GR
184	0°	GR
185	0°	GR
186	0°	GR
187	0°	GR
188	0°	GR
189	0°	GR
190	0°	GR
191	0°	GR
192	0°	GR
193	0°	GR
194	0°	GR
195	0°	GR
196	0°	GR
197	0°	GR
198	0°	GR
199	0°	GR
200	0°	GR

PLY NO.	PLY ORIENT ANGLE	MATERIAL
AIRFOIL	INSERT	
199	0°	GR
200	0°	GR
201	0°	GR
202	0°	GR
203	0°	GR
204	0°	GR
205	0°	GR
206	0°	GR
207	0°	GR
208	0°	GR
209	0°	GR
210	0°	GR
211	0°	GR
212	0°	GR
213	0°	GR
214	0°	GR
215	0°	GR
216	0°	GR
217	0°	GR
218	0°	GR
219	0°	GR
220	0°	GR
221	0°	GR
222	0°	GR
223	0°	GR
224	0°	GR
225	0°	GR
226	0°	GR
227	0°	GR
228	0°	GR
229	0°	GR
230	0°	GR
231	0°	GR
232	0°	GR
233	0°	GR
234	0°	GR
235	0°	GR
236	0°	GR
237	0°	GR
238	0°	GR
239	0°	GR
240	0°	GR
241	0°	GR
242	0°	GR
243	0°	GR
244	0°	GR
245	0°	GR
246	0°	GR
247	0°	GR
248	0°	GR
249	0°	GR
250	0°	GR
251	0°	GR
252	0°	GR
253	0°	GR
254	0°	GR
255	0°	GR
256	0°	GR
257	0°	GR
258	0°	GR
259	0°	GR
260	0°	GR
261	0°	GR
262	0°	GR
263	0°	GR
264	0°	GR
265	0°	GR
266	0°	GR
267	0°	GR
268	0°	GR
269	0°	GR
270	0°	GR
271	0°	GR
272	0°	GR
273	0°	GR
274	0°	GR
275	0°	GR
276	0°	GR
277	0°	GR
278	0°	GR
279	0°	GR
280	0°	GR
281	0°	GR
282	0°	GR
283	0°	GR
284	0°	GR
285	0°	GR
286	0°	GR
287	0°	GR
288	0°	GR
289	0°	GR
290	0°	GR
291	0°	GR
292	0°	GR
293	0°	GR
294	0°	GR
295	0°	GR
296	0°	GR
297	0°	GR
298	0°	GR
299	0°	GR
300	0°	GR



PLY ORIENT ANGLE

LEADING EDGE OF PLY

PLY NO.

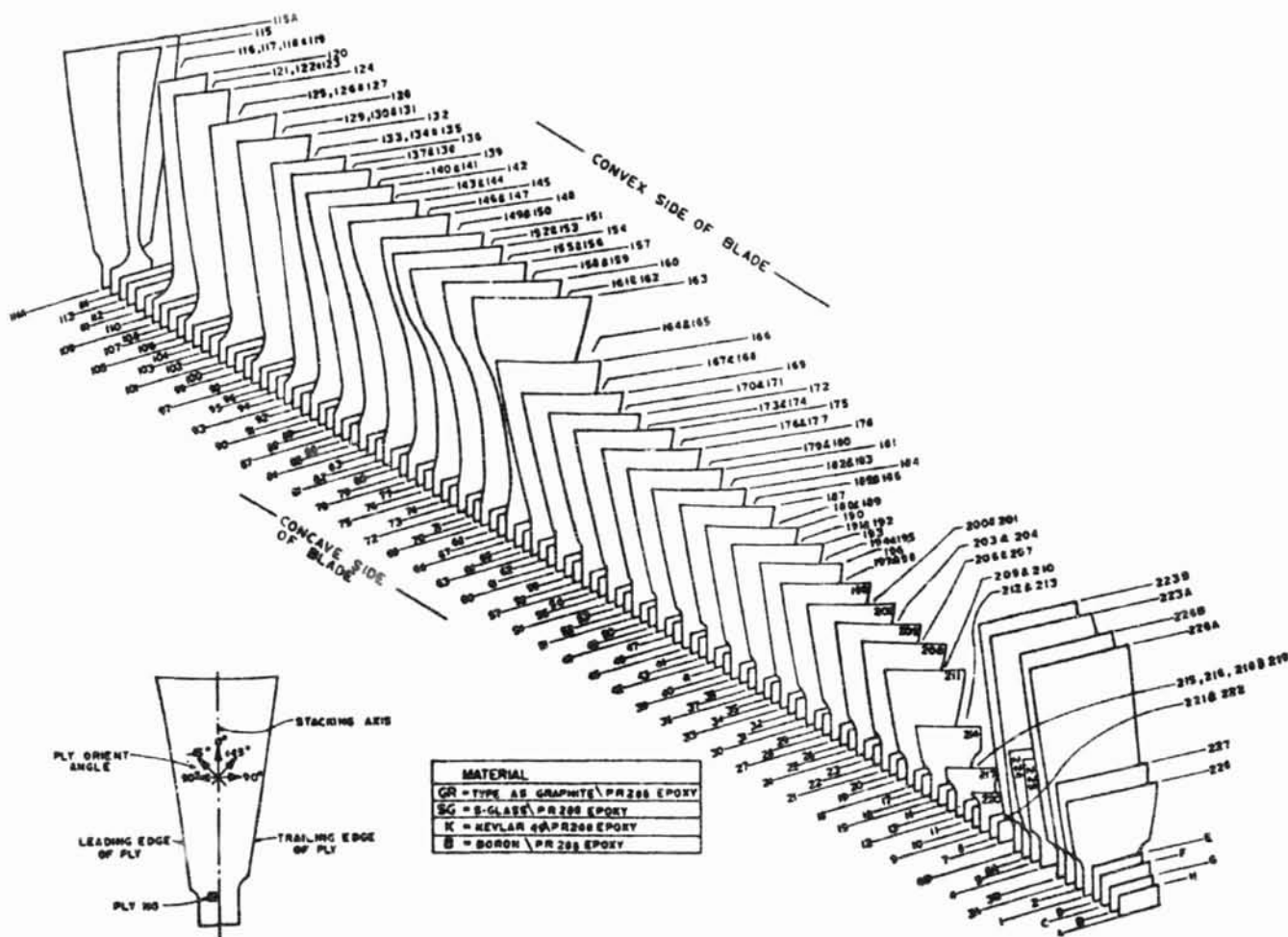
Figure 7. Ply Layup and Material

PRECEDING PAGE BLANK NOT FILMED

FOLDOUT FRAME

PAGE BLANK NOT FILMED

ORIGINAL PAGE IS  
POOR QUALITY



Layout and Material Arrangement.

#### 4.0 FABRICATION

To assure production of high quality blades, a quality control procedure was established. The following paragraphs describe the methods used to assure the required blade-to-blade consistency. All the materials used were procured to General Electric specifications.

##### 4.1 RAW MATERIAL CONTROL

An established quality control plan for inspecting incoming epoxy pre-pregs at General Electric was employed on all materials procured under this program. This plan, which establishes the requirements and methods for selecting satisfactory prepreg material for use in composite blade molding activities, includes the following operations:

1. Checking inventory of incoming material and vendor's certifications for completeness and reported conformance to specification requirements.
2. Logging in each lot and roll received.
3. Visual inspection of workmanship.
4. Sampling of material and verification of compliance with specification requirements, including physical properties, reactivity, and mechanical properties of a molded panel from each combination of fiber and resin batch.
5. Handling, storage, and reinspection of out-of-date materials.
6. Disposition of materials which fail to meet specification requirements.

Specific material properties which were measured and compared to vendor reported data on each prepreg lot are given below:

<u>Prepreg Data</u>	<u>Laminate Data</u>
Fiber, g/m <sup>2</sup>	Flexure str. at RT, 394 K (250° F)
Resin, g/m <sup>2</sup>	Flexure mod. at RT, 394 K (250° F)
Solvent content, % wt	Shear str. at RT, 394 K (250° F)
Gel time, minutes at 383 K (230° F)	Fiber content, % vol
Flow, % wt	Resin content, % vol
Visual discrepancies	Voids, % vol
	Density, g/cc

PRECEDING PAGE BLANK NOT FILMED

## 4.2 BLADE MOLDING

The basic sequence of operations involved in molding the QCSEE composite blades is outlined below. Each blade was layed up in halves and weighed prior to molding. Molding temperature was 383 K (230° F). After cooling and de-flashing, the blades were weighed and density measurements were taken. Along with the blade, go-by test panels were fabricated concurrently to verify mechanical properties.

1. The fully assembled mold tool was heated to the prescribed temperature in the press such that all sections of the die were maintained at a uniform temperature.
2. The press was opened and release agent was applied to the mold cavity surfaces and any excess removed.
3. The assembled blade preform was loaded into the heated mold cavity.
4. The press closed at a fast approach speed until the top and bottom portions of the mold engaged.
5. An intermediate closing speed was selected for preliminary debulking of the blade preform.
6. The dies continued to close at a preselected, slow rate. The movement continued until the die was closed and the prescribed molding load/pressure attained. Figure 8 shows a typical rate of closure and load application curve for molding a PR 288/Type AS composite blade with a gel time of  $60 \pm 5$  minutes at the constant molding temperature 383 K (230° F).
7. The press was opened and the blade molding was rapidly transferred into the postcure oven, thus preventing thermal contraction stresses from being set up in the part. The blade was allowed to hang freely in the postcure oven for the predetermined process time necessary to achieve full material properties.

## 4.3 MOLDING INSPECTION AND FINISHING OPERATIONS

After removing the blades from the postcure oven and trimming the resin flash, the following inspection operations were carried out.

1. Measurement and recording of molded weight, volume and density.
2. Recording of surface defects in sketch form and by photographs taken of both sides of the blade.
3. Dimensional inspection and recording of the root and tip maximum dimensions.

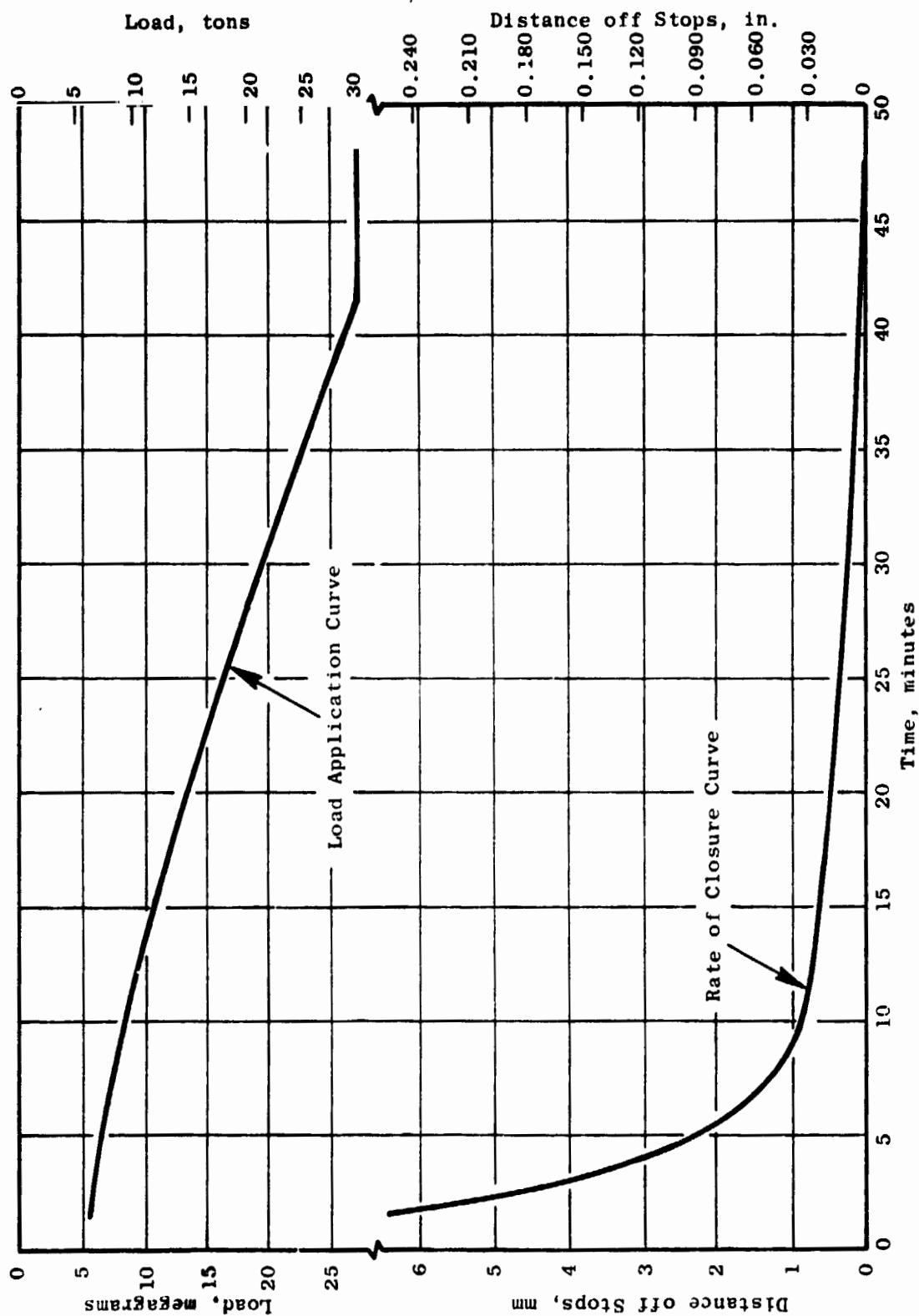


Figure 8. Molding Procedure for PR 288/Type AS Blade with Gel Time at 124 K (230° F).

Although the blade form was molded well within the desired envelope tolerances, it was extremely difficult to mold the dovetail profile to the accuracy required. As a result, dovetail profiles were final machined to size. Foreign object protection systems were also applied to the blade. The principal finishing operations performed on the blades are listed below:

1. Dovetail machining
2. Application of wire mesh to leading edge
3. Application of nickel plating to wire mesh
4. Trimming blade to length and tip forming
5. Outsert installation
6. Platform installation
7. Polyurethane coating

#### 4.4 NONDESTRUCTIVE EVALUATION

All blades manufactured were subjected to through-transmission ultrasonic C-scan (TTUCS) inspection in addition to holographic and root dye penetrant inspection. All blades supplied to verification test and for engine assembly successfully passed these inspections. All verification test blades were also posttest ultrasonically inspected.

##### 4.4.1 Through-Transmission Ultrasonic C-Scan

The test technique, shown in Figure 9, is basically a measurement of sound attenuation due to both absorption and scattering. The through-transmission approach (as opposed to pure pulse-echo or reflection-plate pulse-echo/transmission approaches) provides for a more efficient energy transfer with a minimal influence of test equipment configuration or material/component shape. The scanner contour follows the airfoil with a master/slave servomechanism. Even so, the attenuation values must be referenced to a specific ply stackup and process sequence employed in the manufacture of each component.

High-resolution scanning (50 lines per inch index and 100 pulses per inch scan for 5,000 units of data per square inch), combined with 10 shades-of-gray (5% to 95% on the oscilloscope) recording on dry facsimile paper, provides an "attenugraph" image which is read much in the same manner as a radiograph.



ORIGINAL PAGE IS  
OF POOR QUALITY

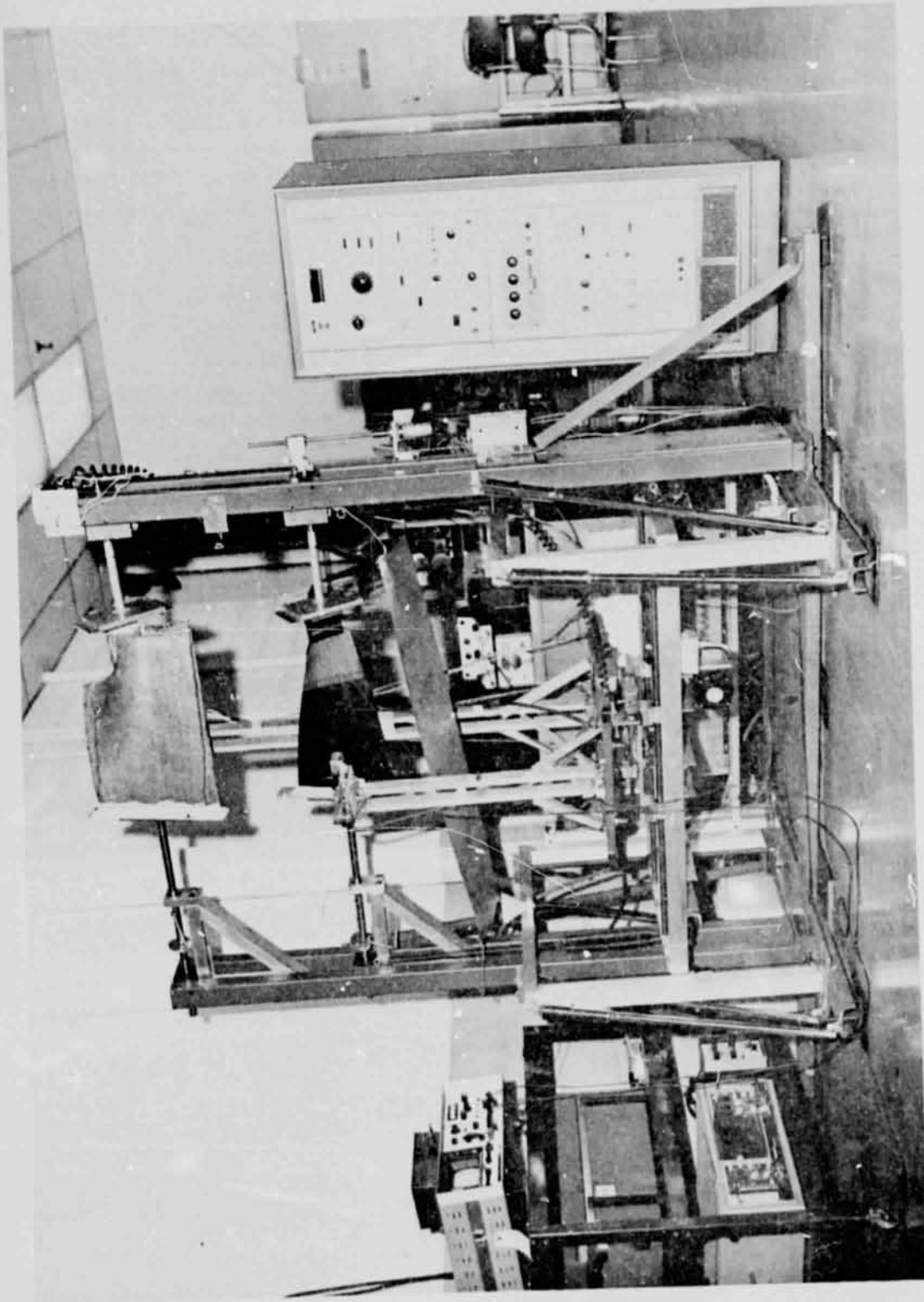


Figure 9. Test Technique for Ultrasonic C-Scan of Composite Blades.

#### 4.4.2 Laser Holographic Interferometry

The laser holographic facility, Figure 10, was also used to inspect the blades molded during this program. It is highly versatile in that the optical devices may be positioned to accommodate a variety of object types and fields of illumination on panels, blades, and other contoured components. Interferometry relies on secure blade fixturing and consistently reproducible stressing for the second exposure of a double-exposure hologram. Typical interferograms are presented in figure 11.

#### 4.4.3 Dye Penetrant Inspection

Dye penetrant inspection of the dovetail area was performed on each of the blades. This test was used to detect surface-connected root delaminations in the machined dovetail. The dye penetrant check also gives qualitative indications of root zone porosity.

ORIGINAL PAGE IS  
OF POOR QUALITY

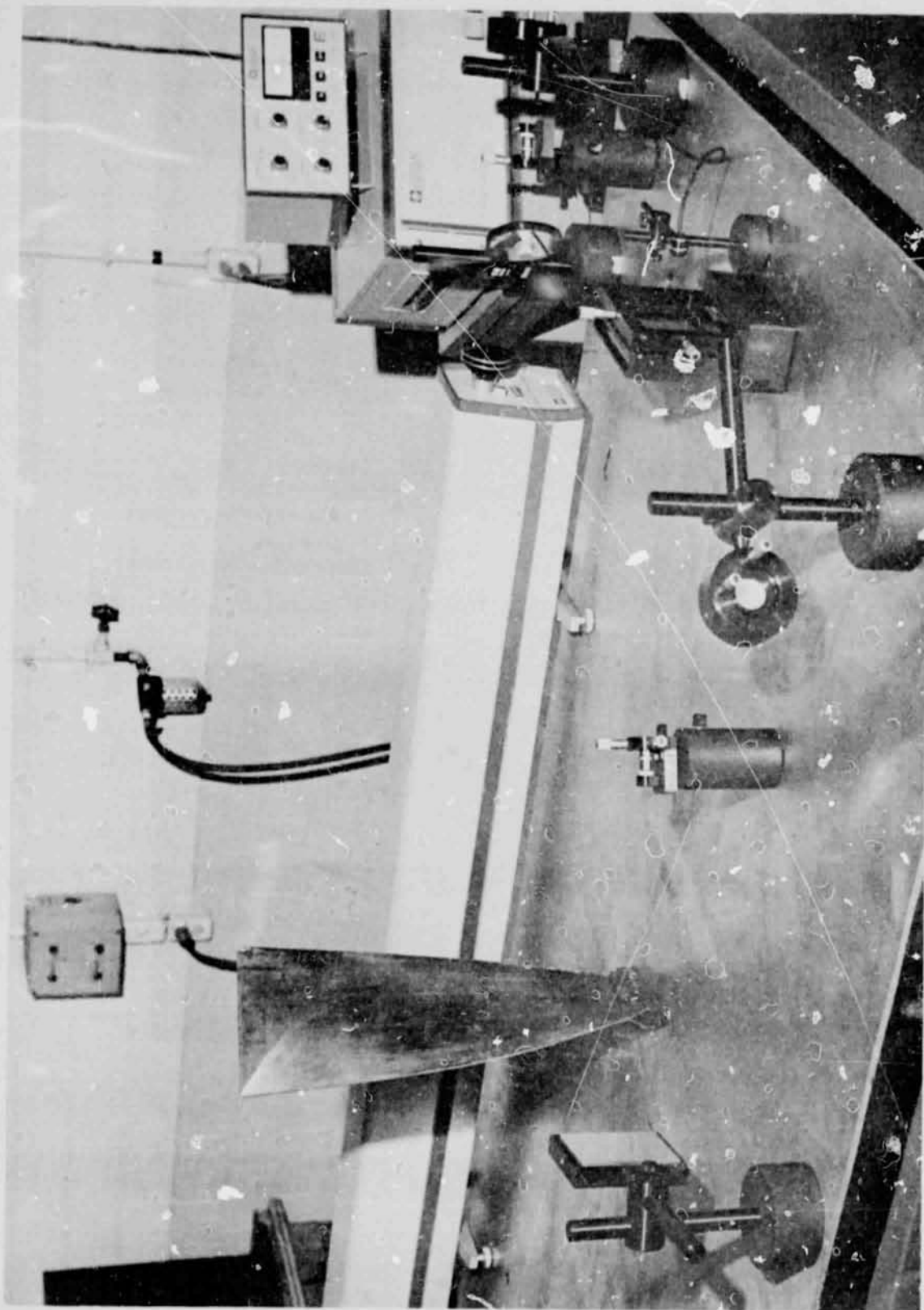


Figure 10. Laser Holographic Facility.



(a) Concave - Tip  
No Discontinuity



(b) Convex - Tip  
Discontinuity at  
LE Caused by Foreign  
Inclusion  
(Cause for Rejection)



(c) Concave - Root  
Slight Discontinuity Due to Ply  
Endings



(d) Convex - Root  
Slight Discontinuity Due to Ply  
Endings

Figure 11. Holograph NDT of QCSEE Blade.

ORIGINAL PAGE IS  
OF POOR QUALITY

## 5.0 UTW COMPOSITE BLADE TESTING

During the final design and manufacturing phase of the program a total of 38 UTW composite blades were manufactured. Twenty-two of these blades were allocated for engine build and spares, five for bench and whirligig testing, and eleven for process and tooling checkout and for verification test backup. One preliminary blade manufactured and tested in the earlier phase of the program was used for platform fabrication and verification testing. Table II summarizes the composite blade tests conducted during this portion of the program.

Whirligig testing is described in Section 6 of this report. Bench testing and results are given as follows:

### 5.1 BLADE FREQUENCY CHARACTERISTICS

Frequency characteristics in the first five modes of vibration were determined for 22 engine blades and 5 test blades. These frequencies were determined to provide a history of each blade's vibratory characteristics and provide backup monitoring of the blade manufacture. The test consisted of clamping the blade's dovetail in a steel holding fixture and exciting the blade using an electromagnetic exciter. Frequencies were determined using an oscilloscope to observe the change in the blade response while varying the frequency of the electromagnet until each of the first five natural frequencies were determined. A summary of the frequency data for each blade is presented in Table III.

This data shows close grouping of the first flexural frequencies but wider variation in the higher mode frequencies. Some of the variation is thought to be attributal to operator techniques since the data from blades tested the same day by a single operator tended to group more tightly than the total body of data. The frequency data agrees with anticipated frequencies for the final blade and is plotted along with whirligig frequency data in Figure 23. The higher value of the bench data from the extrapolated zero speed whirligig data reflects the differences due to the rigid clamping support of the base of the blade.

### 5.2 PLATFORM BENCH TEST

A final design platform was installed on preliminary blade QP004 for combined dynamic fatigue testing of blade and platform together and for static load testing of the platform/blade attachment. The static load test was performed in two phases; the first phase was directed toward determining the load to initiate bond failure at the platform to blade interface and the second phase was to determine the ultimate load capability of the platform for complete separation of a platform from the blade as a means of assessing

Table II. Composite Blade Test Summary.

Test	Blade S/N	Test Summary
1. Frequency Characterization	27 Final Blades With Platforms	Determined 1st 5 model frequencies.
2. Platform Static	QP004	<ul style="list-style-type: none"> <li>• Fatigued in 1st flex to 10% frequency drop.</li> <li>• Loaded at platform max. overhang until bond separated.</li> <li>• Loaded at platform CG to ultimate strength o platform.</li> </ul>
3. Bench Strain Distribution	Q11	<ul style="list-style-type: none"> <li>• Relative stress at first three modes.</li> </ul>
4. Bench Fatigue • 1st Flex	Q9	<ul style="list-style-type: none"> <li>• <math>10^6</math> cycles at <math>159 \text{ MN/m}^2</math> (23 ksi), <math>214 \text{ MN/m}^2</math> (31 ksi), etc., double amplitude stress to 5% frequency drop.</li> </ul>
5. Bench Fatigue • 1st Torsion	Q11	<ul style="list-style-type: none"> <li>• <math>3 \times 10^6</math> cycles at <math>345 \text{ MN/m}^2</math> (50 ksi) and <math>1.4 \times 10^6</math> cycles at <math>448 \text{ MN/m}^2</math> (65 ksi) double amplitude stress.</li> </ul>
6. Whirligig Strain Distribution	Q7	<ul style="list-style-type: none"> <li>• Relative stress at first three modes.</li> <li>• Steady-state stress to 3325 rpm.</li> <li>• Determined Campbell Diagram.</li> </ul>
7. Whirligig LCF	Q7 Q6	1000 cycles, 450 to 3500 rpm. 1000 cycles, 450 to 3500 rpm.
8. Whirligig HCF • 1st Flex	Q7	$3 \times 10^6$ cycles at $122 \text{ MN/m}^2$ (17.7 ksi), $181 \text{ MN/m}^2$ (26.3 ksi) and $253 \text{ MN/m}^2$ (36.7 ksi) and $1.6 \times 10^6$ cycles at $347 \text{ MN/m}^2$ (50.3 ksi).
9. Whirligig Overspeed	Q6	5-1/2 minutes @ 3800 rpm (117% design speed)

Table III. Engine & Test Blade Frequency Inspection Summary.

S/N	Frequency - Zero Speed, Hertz				
	1F <sup>(a)</sup>	2F	1T <sup>(b)</sup>	3F	2T
Q 6	64	186	290	390	610
Q 7	64	194	290	404	616
Q 8	62	184	286	370	602
Q 9	60	194	290	298	618
Q11	62	192	290	396	612
Q12	60	178	282	356	596
Q14	61	186	286	382	612
Q15	62	186	286	380	610
Q17	62	180	282	364	602
Q18	62	180	284	358	602
Q19	62	180	284	358	598
Q20	62	188	288	382	612
Q21	62	182	282	364	598
Q22	62	182	282	364	602
Q23	61	186	286	378	608
Q24	61	188	284	380	608
Q25	60	182	284	360	600
Q26	62	180	282	360	594
Q27	62	188	286	380	610
Q28	62	178	282	354	594
Q29	62	180	284	354	602
Q31	62	182	284	360	600
Q32	62	180	282	360	592
Q34	62	180	282	354	590
Q36	62	188	288	380	616
Q37	62	180	284	358	600
Q38	62	180	282	360	596
(a) Flexural Mode (b) Torsional Mode					

the fail/safe capabilities of the platform after disbonding. Wrap around straps (at the leading and trailing edges of the blade) incorporated in the platform's design are intended to provide the platform with the required structural capability even with a debond between blade and platform. The leading edge strap is shown in Figure 5.

Prior to fabrication of the platform on Blade QP004, this blade had been previously subjected to first torsional fatigue testing in the Whirligig, which had fatigue damaged the blade to the extent that the first torsional frequency was reduced approximately 10% during that test. That damage was internal to the blade and did not affect the platform's fabrication.

The blade with platform was subjected to bench fatigue testing by exciting it in its first flexural mode, similar to the testing described in Section 5.4. It was tested until its first flexural frequency was reduced by 10% which occurred after one million cycles at  $193 \text{ MN/m}^2$  (28 ksi) double amplitude stress and 0.5 million cycles at  $241 \text{ MN/m}^2$  (35 ksi) stress. This caused approximately 50% debond at the platform to blade interface surface. The blade was next prepared for static load testing by potting the airfoil into a Devcon block for support.

The static load testing consisted of evaluating the load-deflection capability of the platform and determining the load required to totally separate the platform from the blade. A point static loading was used to simulate centrifugal loading. The setup is shown in Figure 12. An Instron testing machine applied an equal compressive load to the bottom of each side of the platform. The load was applied near the platform maximum overhang. Loading was stopped prior to failure of the end straps that retain the platform to the blade. Next, the load was repositioned to bear on the centrifugal loading center of pressure for each half platform and the loading continued until the end straps failed and the platform halves separated from the blade. A test load of 8.0 kN (1800 lb) applied at the platform maximum overhang position caused bond separation of platform from blade. Figure 13 shows a plot of the platform deflection as a function of this loading. A final test load of 17.1 kN (3850 lb) applied at the center of pressure of the half platforms caused the end straps to break and the platform halves to separate from the blade.

The total operating centrifugal load of the platform is calculated to be 5.3 kN (1200 lb) acting at the platform CG. The test load of 8.0 kN (1800 lb) applied at the maximum overhang position and required to cause bond separation shows a margin of safety of over 2.0 on this loading when considered on an equivalent moment basis. The load of 17.1 kN (3850 lb) applied at the center of pressure of the platform shows a margin of safety of over 2.0 on the capability of the end straps to retain the platform on the blade in the event of the platform debonding from the blade. These margins demonstrate that the platform is satisfactory for engine operation.



ORIGINAL PAGE IS  
OF POOR QUALITY

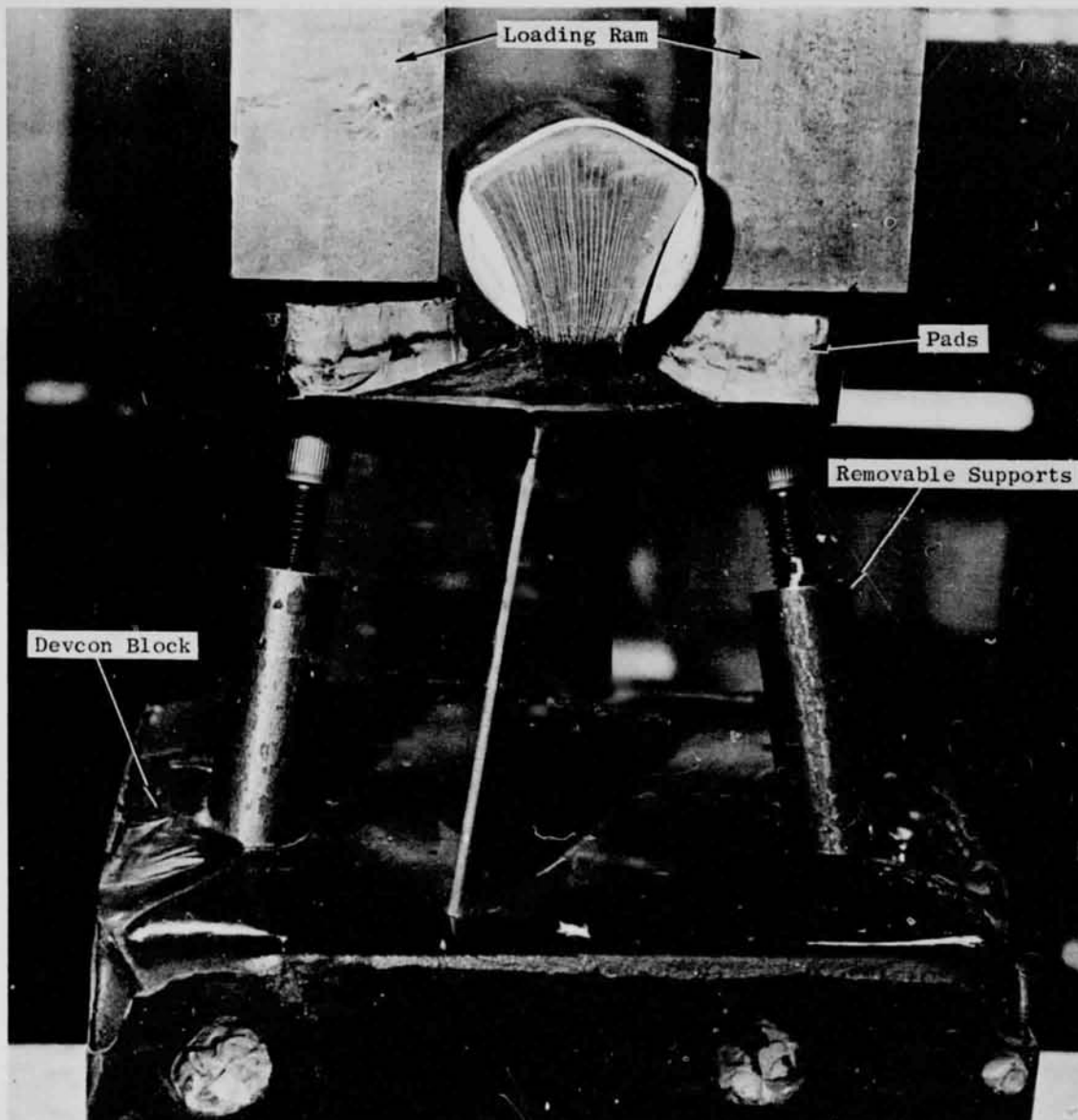


Figure 12. Blade Platform Load Test Setup (C7507477).

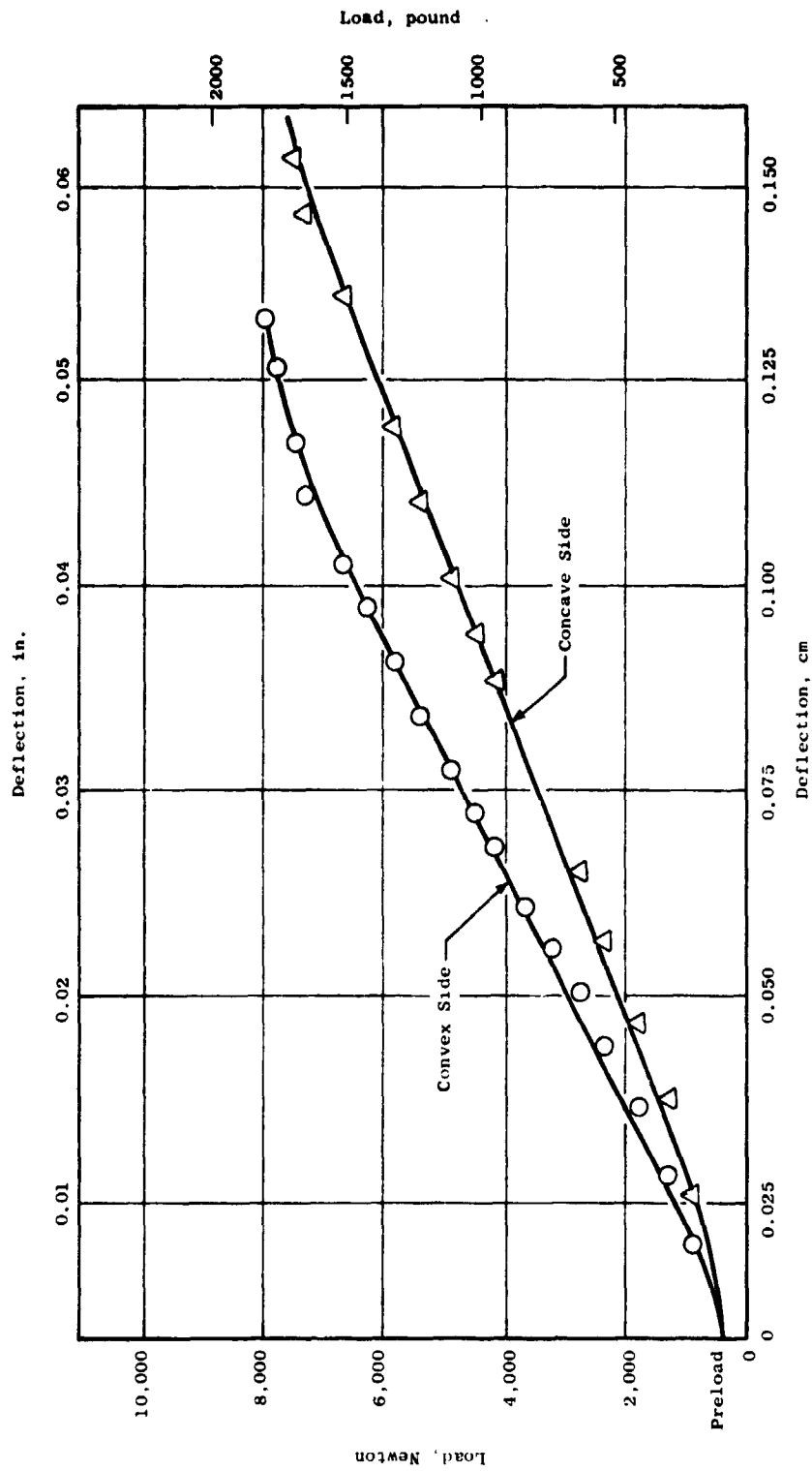


Figure 13. Platform Load Test Deflections.

### 5.3 BENCH STRAIN DISTRIBUTION

A bench strain distribution test was performed on blade Q11 for the purpose of determining the strain distribution in the first five natural modes of vibration. This data is useful in assessing relative vibratory stresses of the blade in conjunction with engine testing. Areas of maximum vibratory stress are combined with steady state stresses to set the limits for engine operation.

The strain distribution test was run using a siren facility which produces pulses of air that impinge on the blade to excite the blade at a constant force, on resonance, while strain gage readouts were recorded. The blade was instrumented with 42 strain gages as shown in Figure 14. Since this blade included a platform which covers the airfoil to root transition region, the stresses in this region could not be directly measured. Data from preliminary blade testing were used along with the data from this test to determine the actual maximum stresses which in some cases are located under the platform.

In order to ensure that no damage to the blade occurred during strain distribution testing, the levels of excitation were kept well below the fatigue limits of the blade. The two levels of strain used during testing were 625 and 1250  $\mu$  cm/cm as measured at the maximum gage location. Strains at all gage locations were recorded as a percentage of the strain at the maximum gage location.

Table IV tabulates this data for the first five natural frequencies. The data shows that at the first flexural mode, the maximum measured strain location is on the convex midchord region of the blade immediately above the platform. Generally, the highest stresses were measured on the blade airfoil near the platform on both the concave and convex sides. The second flexural mode showed some shift in the maximum stress location but a very similar response of highest stresses in the airfoil near the platform. The maximum measured strain location in the first torsional mode was at the blade trailing edge on the convex side slightly above the platform. Considerably higher torsional stresses are expected at the root trailing edge undercut region as shown in the preliminary design test report, Reference 2. This was taken into consideration in assessing fatigue test results. The relative strains for the fourth and fifth modes are also included in Table IV for reference purposes.

### 5.4 BENCH FATIGUE TESTS

Bench high cycle fatigue tests were performed on blades Q9 and Q11 to determine the blades' alternating stress capability. Q9 was tested at its first flexural natural frequency and Q11 at its first torsional natural frequency. Both blades were complete with platforms. The tests were performed by clamping the blade dovetail in a rigidly supported holding fixture, and exciting the blade. Excitation was provided by a siren facility which pro-

Gage No.	Direct.	Location	
		Y	Z
1	90°	Noted	12.7 cm (5.0 in.)
2	90°	Noted	10.16 cm (4.0 in.)
3	90°	Noted	Noted
4	45°	Noted	Noted
5	0°	Noted	Noted
6	90°	5.97 cm (2.35 in.)	Noted
7	90°	5.33 cm (2.10 in.)	Noted
8	90°	3.68 cm (1.45 in.)	Noted
9	90°	2.29 cm (0.90 in.)	Noted
10	90°	0.64 cm (0.25 in.)	Noted
11	90°	-1.27 cm (-0.50 in.)	Noted
12	90°	-3.30 cm (-1.30 in.)	Noted
13	90°	-5.33 cm (-2.10 in.)	Noted
14	45°	-5.33 cm (-2.10 in.)	Noted
15	0°	-5.33 cm (-2.10 in.)	Noted
16	90°	Noted	Noted
17	90°	3.81 cm (1.50 in.)	5.59 cm (2.2 in.)
18	90°	1.52 cm (0.60 in.)	5.84 cm (2.3 in.)
19	90°	-1.02 cm (-0.40 in.)	5.84 cm (2.3 in.)
20	90°	-3.56 cm (-1.40 in.)	6.10 cm (2.4 in.)
21	90°	Noted	12.7 cm (5.0 in.)

ORIGINAL PAGE IS  
OF POOR QUALITY

(Gages are back-to-back on Concave, CC,  
and Convex, CX, sides)

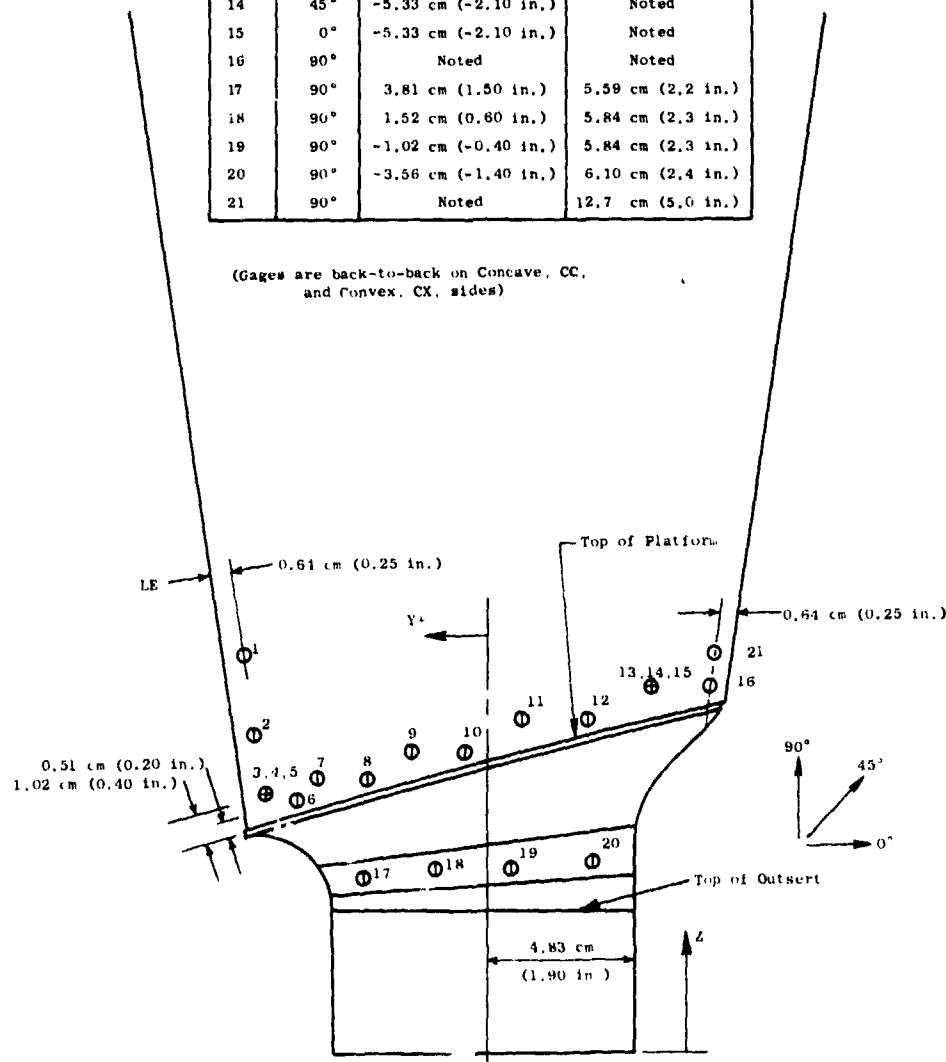


Figure 14. Bench Test Blade Instrumentation, Blade S/N Q11.

Table IV. Bench Test Relative Strain Distribution - Blade Q11.

Strain Gage Number Concave Side	Relative Strain, %					Strain Gage Number Convex Side	Relative Strain, %				
	1F (a)	2F	1T (b)	3F	2T		1F	2F	1T	3F	2T
01	40	46	23	38	13	01	18	52	26	38	25
02	37	48	1	33	21	02	14	31	21	41	31
03	27	36	11	21	13	03	5	22	25	12	36
04	2	2	6	11	12	04	8	9	11	12	11
05	15	18	3	12	15	05	5	4	14	16	10
06	44	73	80	56	41	06	2	25	73	73	76
07	51	83	58	71	22	07	16	11	37	76	61
08	36	65	74	61	33	08	53	19	43	100	100
09	33	50	46	31	22	09	51	32	12	48	52
10	39	50	49	16	43	10	100	95	15	28	76
11	33	29	14	21	38	11	46	56	2	22	21
12	41	28	25	44	43	12	51	100	25	93	12
13	30	23	57	35	26	13	13	5	9	35	20
14	5	12	86	16	11	14	18	13	61	15	11
15	13	4	47	36	16	15	2	38	5	61	15
16	17	27	90	14	13	16	29	2	19	46	9
17	29	58	19	53	31	17	17	15	5	26	43
18	11	16	5	12	18	18	16	19	2	7	26
19	15	15	6	13	26	19	11	15	3	9	15
20	8	7	2	16	16	20	11	21	2	16	15
21	32	28	70	26	12	21	23	6	100	51	5

(a) Flexural Mode

(b) Torsional Mode

duces pulses of air that are directed at the blade. The frequency and magnitude of the pulsating force is regulated until the desired resonant frequency is in the natural mode of interest.

Test stress levels were selected in an attempt to identify the runout fatigue strength with no frequency drop and also to identify the stress level and number of cycles corresponding to a 5% frequency drop. Blade Q9 was instrumented with eight single-element and one three-element rosette strain gages. Gages were located as shown in Figure 15. Strain gage location was based on strain distribution tests whereby areas of max strain are identified in each vibrational mode of interest. Tip deflection and strain gage readings were monitored while the blade was being excited. The maximum tip deflection at the trailing edge of the blade was maintained constant during each portion of the test and used as the control. This procedure is used, based on experience which has shown that strain gages have limited cyclic life and could fail before completion of the test. For blade Q9, the initial peak double amplitude stress was set at  $159 \text{ MN/m}^2$  (23 ksi DA) at its maximum stress location for excitation is the blades first flexural mode. The maximum stress location was identified by analysis and strain distribution test to be on the convex side of the blade near the midchord location just above the platform. Measured strains in the blade spanwise direction have been used to calculate stresses using a material Modulus of Elasticity of  $10 \times 10^6$  psi. This provides a consistent basis for comparing stresses during these tests as well as for setting scope limits and gage monitoring during later engine testing. Runout at each cyclic level of stress was one million cycles. Double amplitude stress increases of  $55 \text{ MN/in}^2$  (8 ksi) were used for subsequent levels of testing. Testing was continued until a 5% drop in blade frequency occurred. The results of this test are summarized in Table V. This testing shows that the blade can be subjected to a first flexural vibratory double amplitude max stress in excess of  $207 \text{ MN/in}^2$  (30 ksi) with no loss in frequency.

Blade Q11 was instrumented for strain distribution testing as described in Section 5.3. After completion of the strain distribution testing, the blade was bench fatigue tested in its first torsional mode. During fatigue testing gage No. 21CX on the convex side at the trailing edge slightly above the platform was the primary gage monitored (see Figure 14). It was determined from preliminary blade testing that the blades critical stress locations in first torsional mode was at the concave side trailing edge root undercut region. This region could not be strain monitored on blade Q11 since it is covered by the platform. Correlation of blade Q11 strains with those from preliminary blades shows stresses at gage No. 21CX to be at approximately 50% of the blades maximum stress. The trailing edge tip deflection was also monitored during fatigue testing to provide a relationship between strain and tip displacement to be used in the event the strain gages went out during testing.

The results of this are as follows:

ORIGINAL PAGE IS  
OF POOR QUALITY

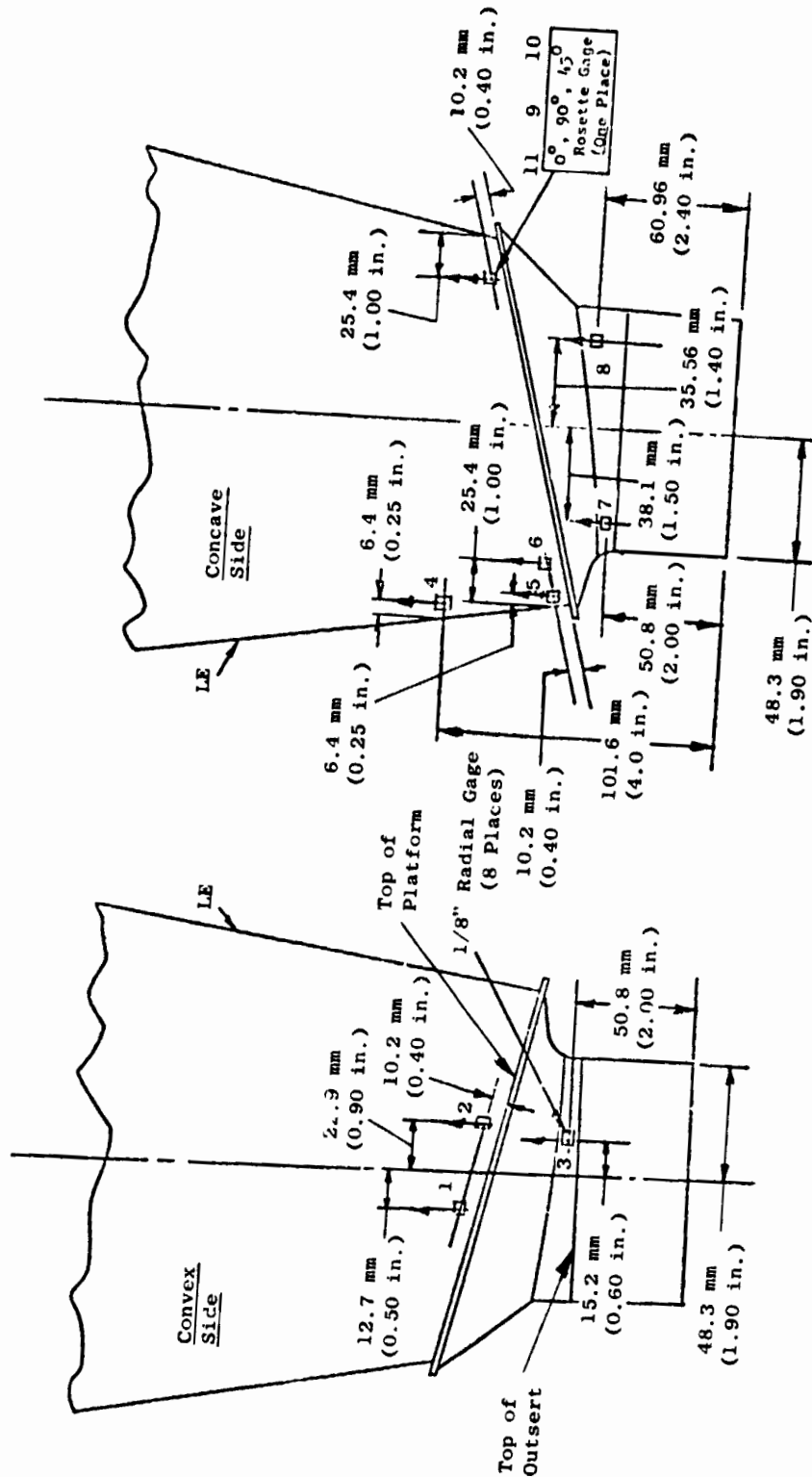


Figure 15. Bench Fatigue Test Instrumentation, Blade S/N Q9.

Table V. Bench First Flexural High Cycle Fatigue Test Summary, Blade Q9.

Double Amplitude Max Stress		Trailing Edge Tip Deflection		No. of Cycles $\times 10^6$	Frequency Hertz	
MN/m <sup>2</sup>	(ksi)	cm	(inch)		Start	End
159	(23)	0.88	(0.345)	1.0	63	63
214	(31)	1.18	(0.465)	1.0	63	63
262	(38)	1.45	(0.570)	1.0	63	63
317	(46)	1.75	(0.690)	1.0	63	62
372	(54)	2.06	(0.810)	1.0	62	61
427	(62)	2.36	(0.930)	0.16	61	60



- $3 \times 10^6$  cycles at  $345 \text{ MN/m}^2$  (50 ksi) double amplitude stress at the trailing edge undercut, with trailing edge tip double amplitude deflection of 1.3 cm (0.510 inch). The frequency dropped from 289 Hz to 279 Hz (3-1/2%).
- Followed by  $1.4 \times 10^6$  cycles at  $448 \text{ MN/m}^2$  (65 ksi) double amplitude stress trailing edge tip deflection was 1.6 cm (0.630 inch) and frequency dropped from 279 Hz to 274 Hz at which point the test was stopped.

The results of this test show that some loss in blade frequency occurs from a first torsional vibratory double amplitude stress of  $345 \text{ MN/m}^2$  (50 ksi). An extrapolation of the data indicates that below a stress limit of approximately  $207 \text{ MN/m}^2$  (30 ksi) double amplitude, no loss in frequency would occur in the first torsional vibratory condition.

Damage in both blades Q9 and Q11 consisted of delamination in the blade airfoil to root transient area and some debonding of the platform's lower attachment. Figure 16 shows the result of ultrasonic and die penetrant examination of the root and dovetail of blade Q9 and Figure 17 shows this for blade Q11.

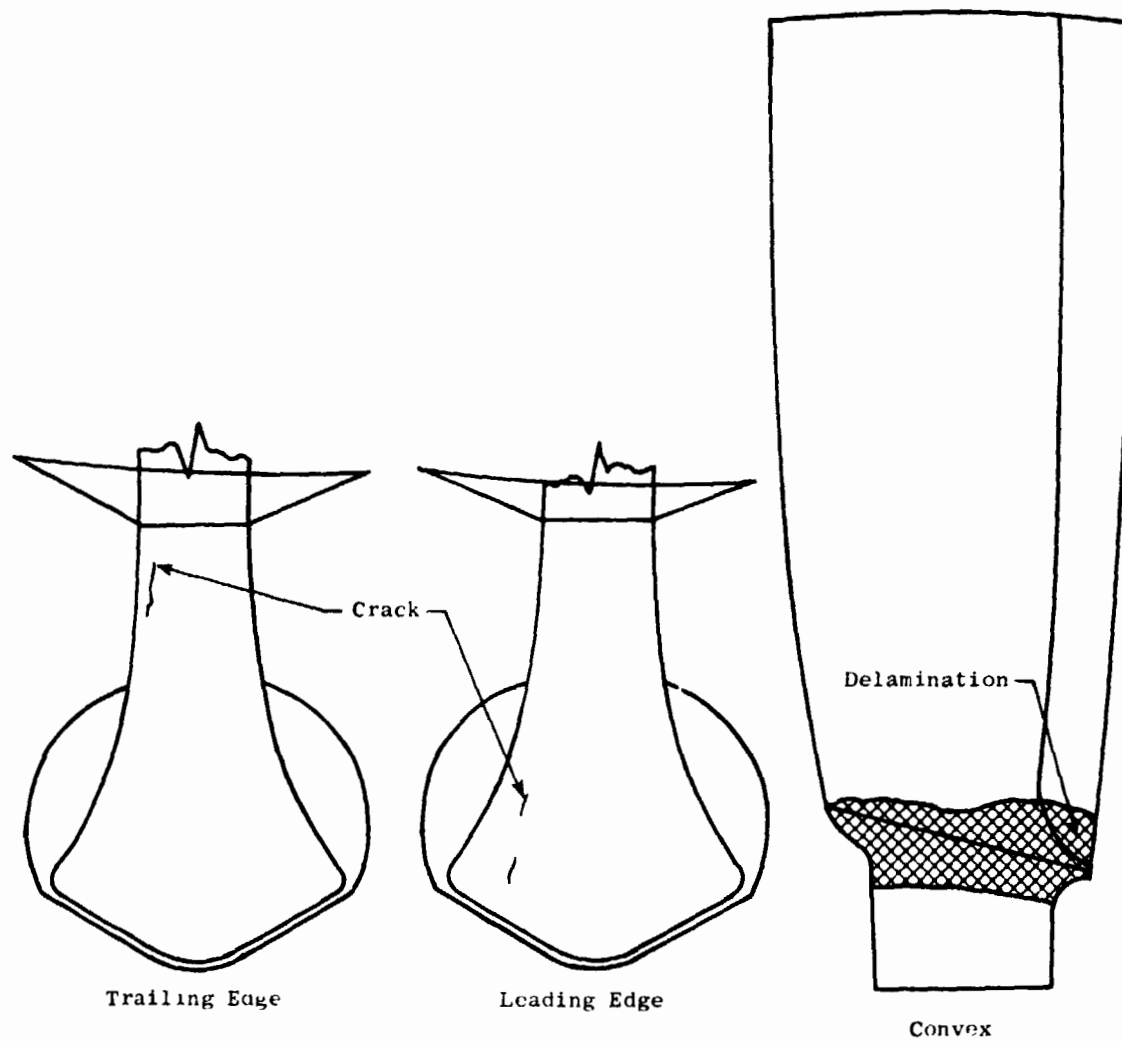


Figure 16. Posttest Evaluation, Blade S/N Q9.

ORIGINAL PAGE 15  
OF POOR QUALITY

ORIGINAL PAGE IS  
OF POOR QUALITY

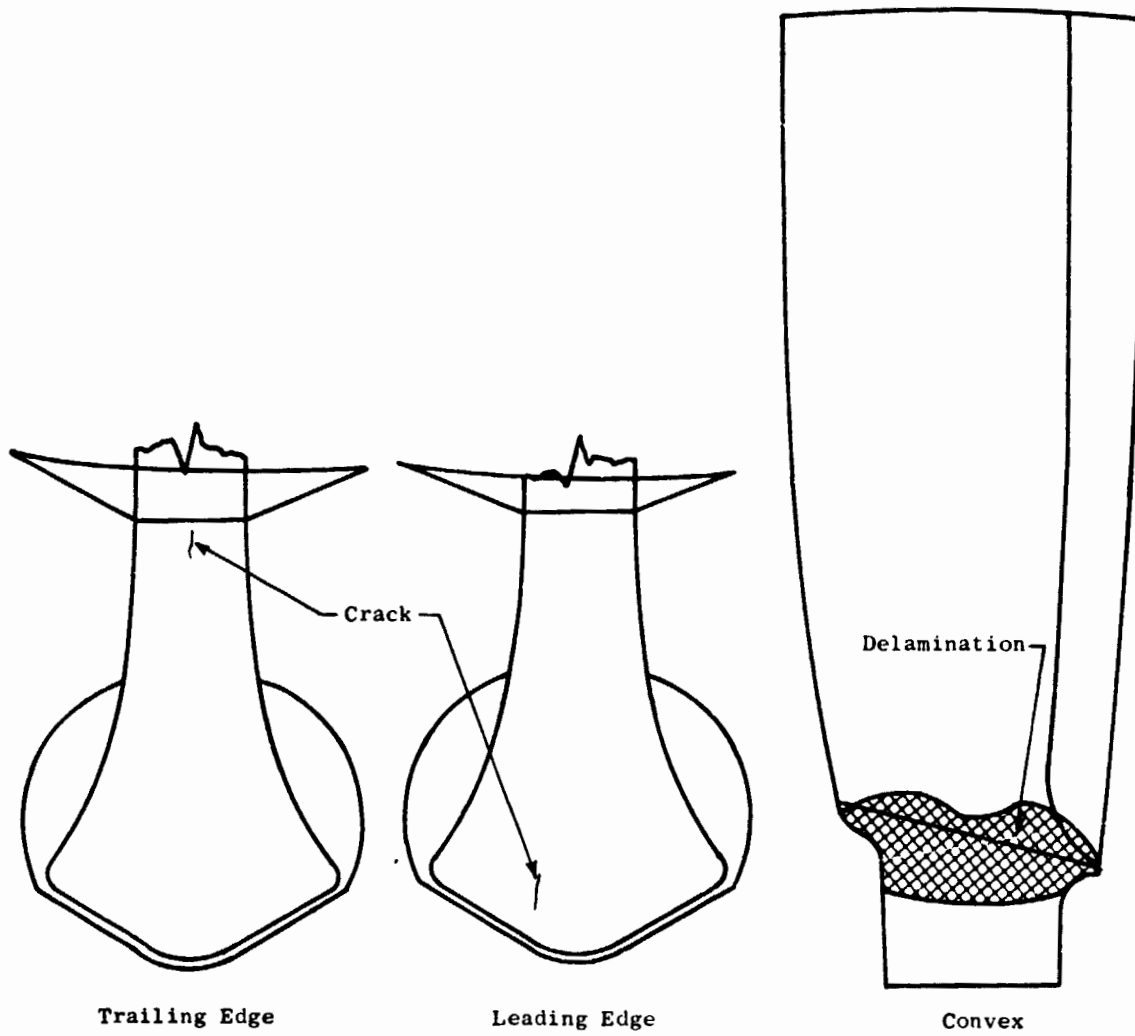


Figure 17. Posttest Evaluation, Blade S/N Q11.

## 6.0 WHIRLIGIG TESTING

As a means of evaluating the strength capabilities of the QCSEE composite blade under simulated engine operating conditions, several whirligig tests were conducted. These tests were conducted on two blades (complete with platforms) and are summarized as follows:

- Whirligig Dynamic Strain Distribution - S/N Q7
- Whirligig Steady-State Strain Distribution - S/N Q7
- Cyclic Testing - S/N Q6 and Q7
- Overspeed Testing - S/N Q6
- Whirligig High Cycle Fatigue - S/N Q7

All 22 blades allocated for engine use were also individually proof-tested in the whirligig prior to delivery for engine buildup.

### 6.1 WHIRLIGIG STRAIN DISTRIBUTION

The objective of this test was to obtain relative dynamic and steady-state strain levels in several locations on the blade during rotating whirligig testing. This was accomplished using blade Q7 which was instrumented as defined in Figure 18. A total of 11 single-element strain gages were used for recording dynamic strains. Four of these gages were designed to provide steady state (absolute strain level) as well as dynamic strains.

The Whirligig facility used for this testing is shown in Figure 19. A cover plate in front of the rotor and feed-in for the airlines used in the dynamic strain testing are also seen. Figure 20 shows the assembled blade, trunnion and disk in the facility prior to installation of instrumentation wiring. Figure 21 shows the setup with the cover plate installed and instrumentation wiring on the blade, trunnion and disk.

For the dynamic strain distribution determination, the instrumented blade was excited in the first three modes of vibration by injecting air through ports in the plate in front of the rotor. The excitation forces and resulting strain level were obtained by increasing the air pressure through the nozzles.

Figure 22 shows the predicted Campbell diagram for the blades and the points on the diagram used for determining the dynamic strain distributions. The test consisted of making medium rate accelerations of approximately 2000 rpm/min to 3326 rpm for per-rev conditions of 2/rev, 3/rev, 4/rev, 6/rev and 9/rev. The speed was held at each resonant peak for short periods of time (approximately five seconds) to obtain the frequency content on the tape recorder. The excitation air was adjusted for each condition so that no gage

ORIGINAL PAGE IS  
OF POOR QUALITY

Gage No.	Y	Z
SS01CX	-1.27 cm (-0.50 in.)	5.08 cm (2.00 in.)
TK01CX	-2.54 cm (-1.00 in.)	5.08 cm (2.00 in.)
SS02CC	-3.68 cm (-1.45 in.)	5.08 cm (2.00 in.)
TK02CC	-2.79 cm (-1.10 in.)	5.08 cm (2.00 in.)
SS03CC	3.56 cm (1.40 in.)	6.10 cm (2.40 in.)
TK03CC	2.54 cm (1.00 in.)	6.10 cm (2.40 in.)
SS04CC	Noted	Noted
TK04CC	Noted	Noted
SD05CC	Noted	Noted
SD06CC	Noted	10.16 cm (4.00 in.)
SD07CC	Noted	Noted
SD08CC	Noted	Noted
SD09CC	Noted	23.88 cm (9.40 in.)
SD10CX	-2.29 cm (-0.90 in.)	Noted
SD11CX	1.27 cm (0.50 in.)	Noted
TK12CX	0	Noted
TK13CX	3.45 cm (1.36 in.)	35.31 cm (13.90 in.)

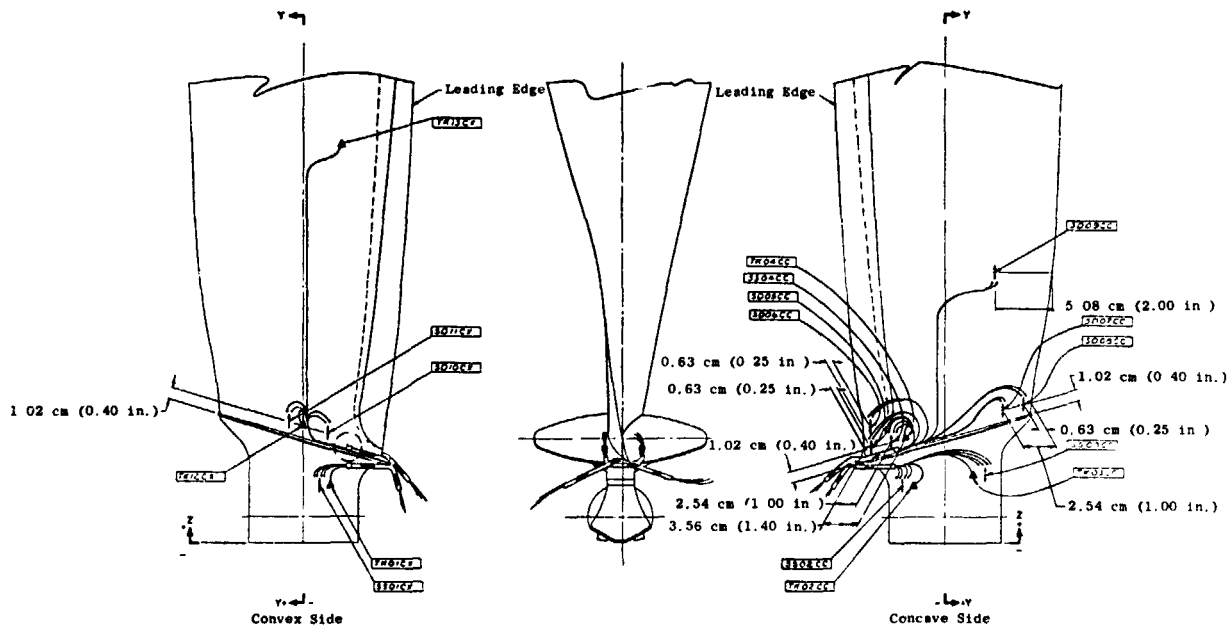


Figure 18. Whirligig Test Blade Instrumentation, Blade S/N Q7.

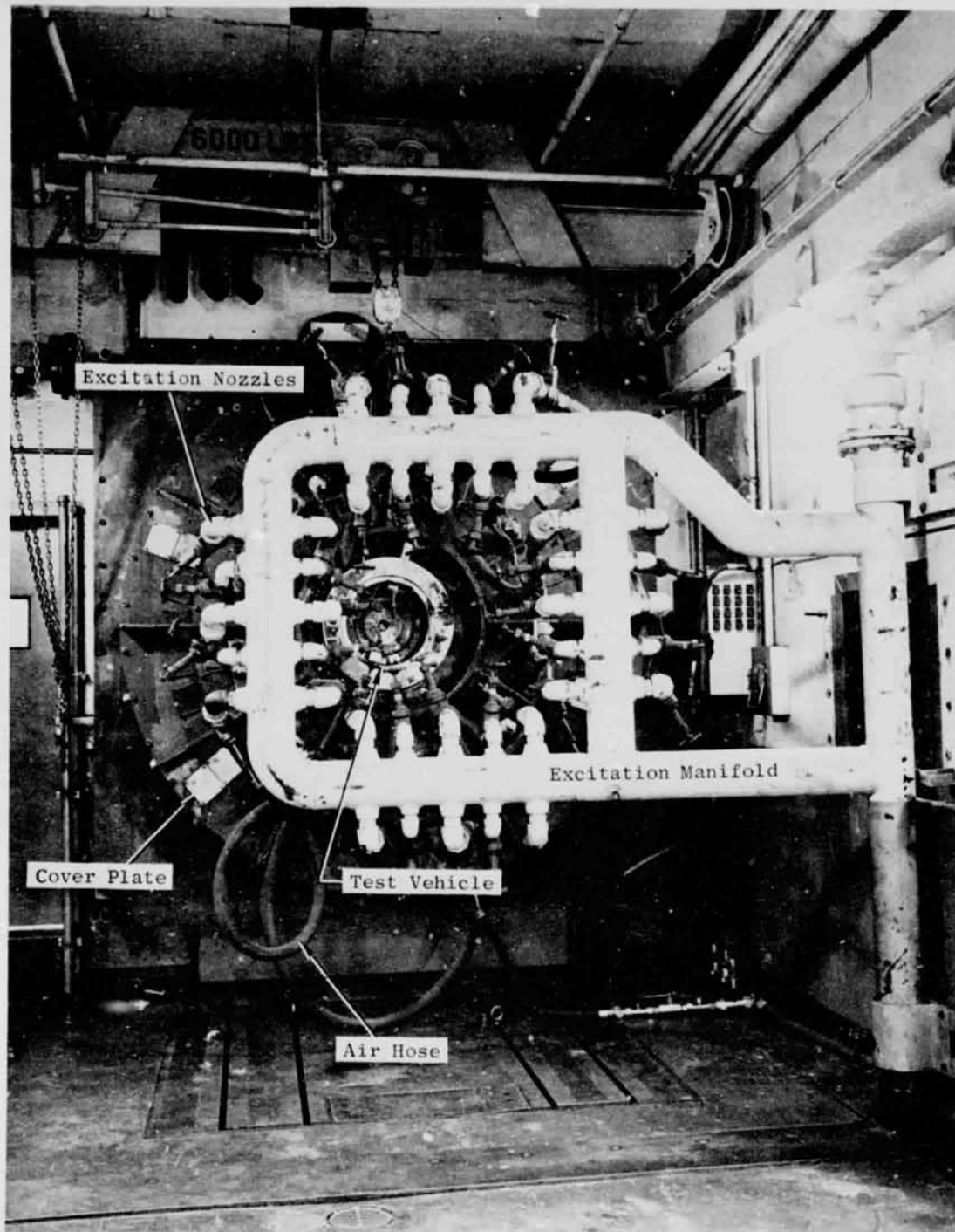


Figure 19. Whirligig Facility Test Cell (C7601185).

ORIGINAL PAGE IS  
OF POOR QUALITY

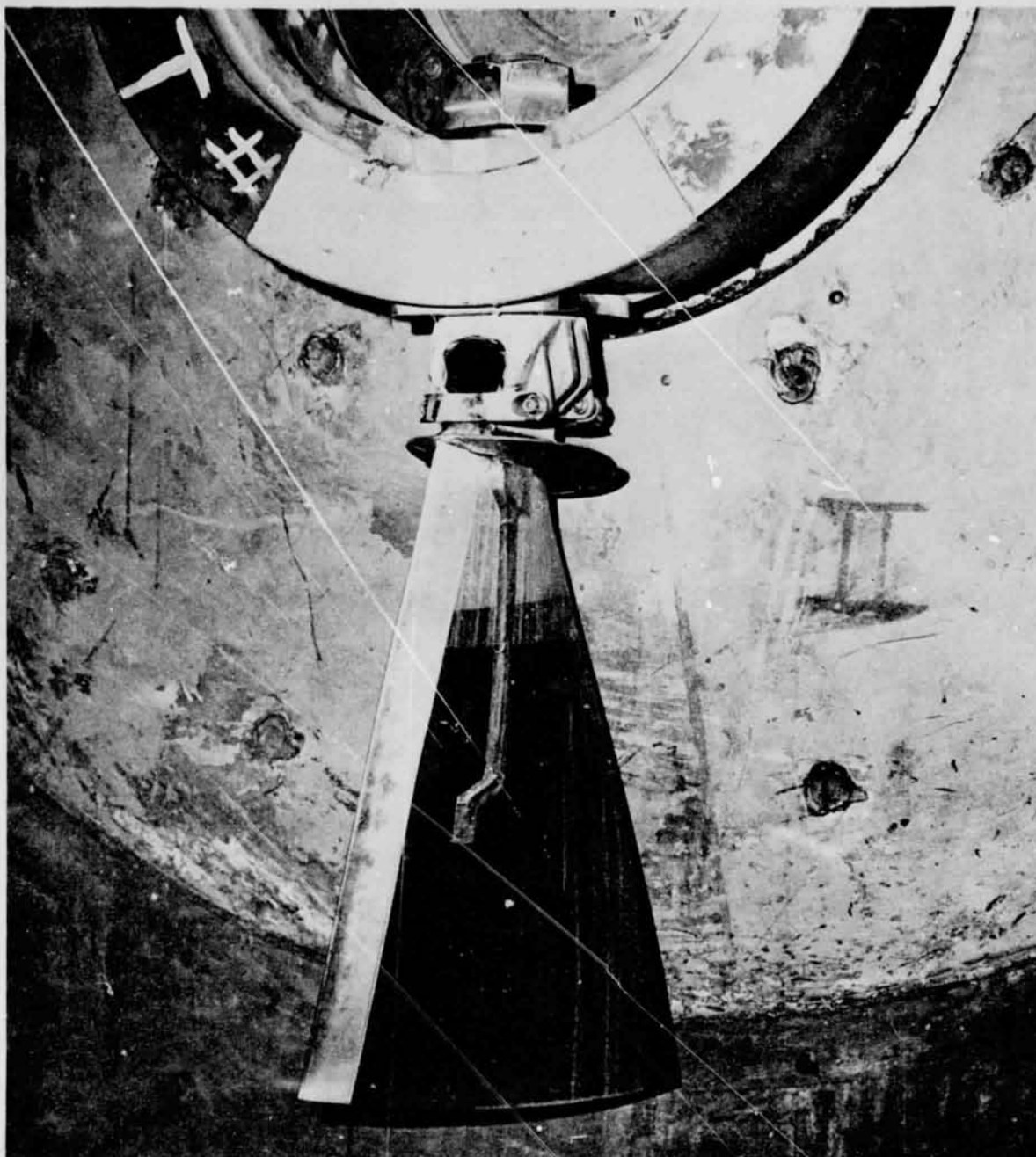


Figure 20. Assembled Blade, Trunnion and Disk (C7601750).

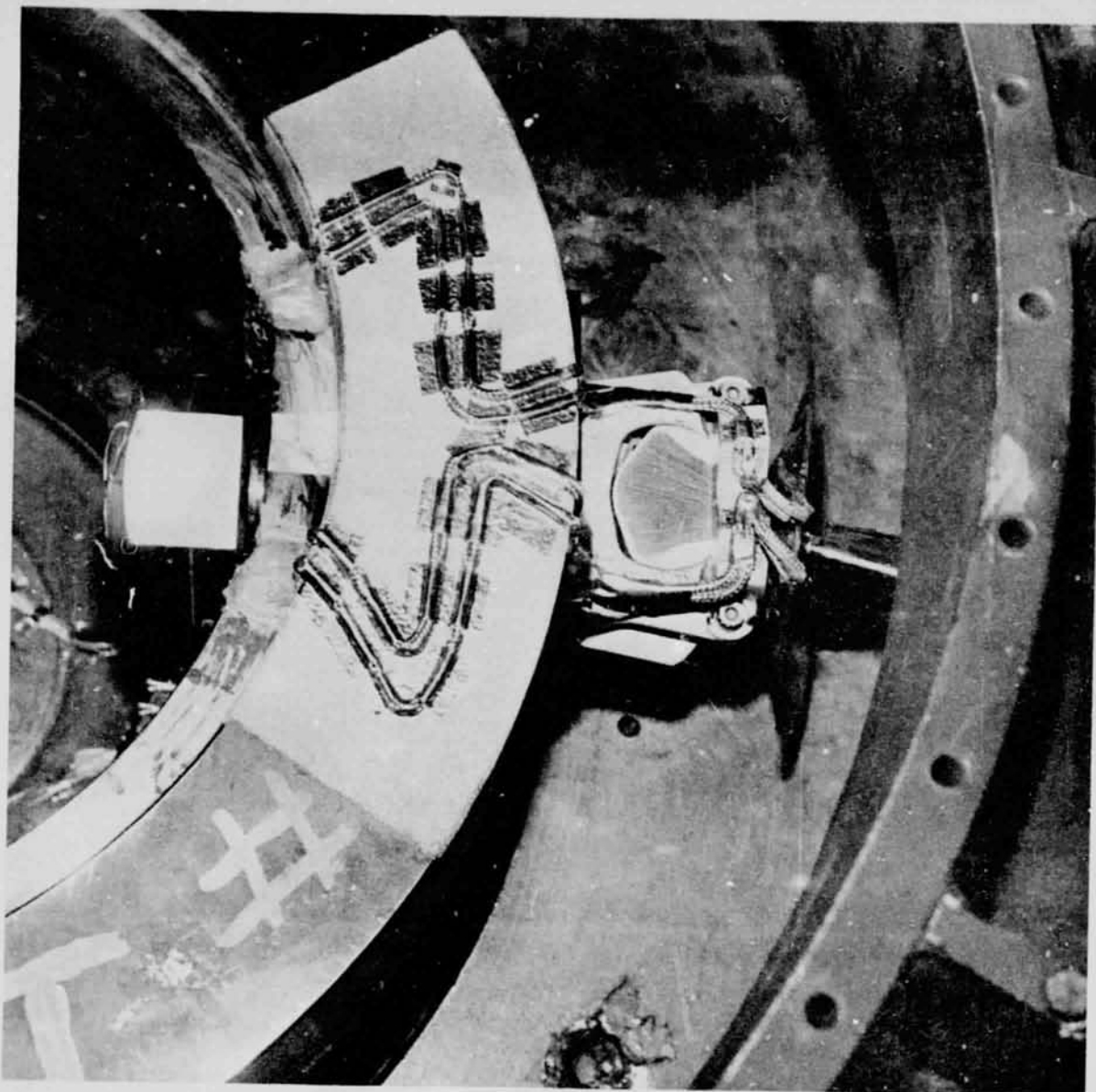


Figure 21. Whirligig Test Instrumentation Leadout C7601337).



ORIGINAL PAGE IS  
OF POOR QUALITY

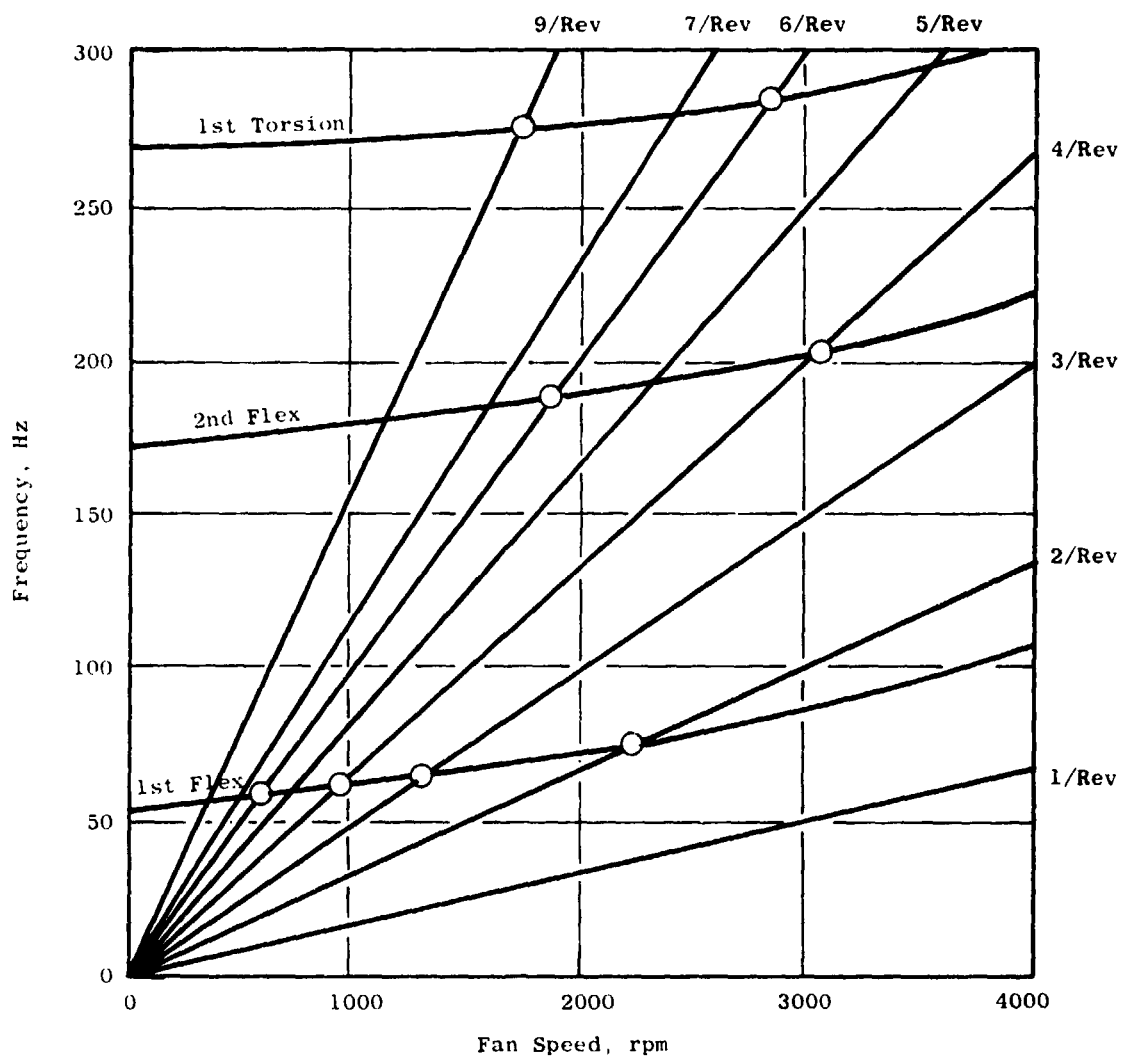


Figure 22. Predicted Campbell Diagram, QCSEE UTW Fan Blade.

responded to more than  $69 \text{ MN/m}^2$  (10 ksi) during this portion of the strain distribution testing. During this portion of the testing, the rotor was run opposite to the normal engine direction to impart maximum energy to the blade. This allowed air excitation nozzles to be directed perpendicular to the blade with the maximum relative velocity between the air and the blade. Table VI lists the results of this test in the form of relative strain levels for each gage in the 1F, 2F and 1T modes. In the first flexure mode, the highest stress readings were obtained from gages SS01CX, SS02CS and SD10CX. Gages SS01CX and SS02CX were on the blade root quite close to the outsert, 5.08 mm (0.20 in.) above the outsert, and are influenced by localized higher strains. Gage SD10CX was near the midchord convex side and is considered the most meaningful gage for blade monitoring purposes.

Table VI. Whirligig Strain Distribution.

Strain Gage No.	Relative Dynamic Strains, %		
	1F(a)	2F	1T(b)
SS01CX	133	43	17
SS02CC	100	100	83
SS03CC	0	0	0
SS04CC	16	14	53
SD05CC	71	53	53
SD06CC	71	66	0
SD07CC	49	14	67
SD08CC	44	29	100
SD09CC	27	29	0
SD10CX	100	23	0
SD11CX	89	63	0

(a) Flexural Mode

(b) Torsional Mode

The higher stresses in the root near the outsert were not originally anticipated. Strain gages on the preliminary blades had not been placed as close to the outsert and did not measure these high stresses. Results of more recent analysis and testing on another program show this phenomena to be a localized stress concentration effect. Although these stresses are higher than anticipated, they are still less than the maximum stress determined for the airfoil convex side midchord location (using the data from the bench strain distribution) 1F test (Table IV). For the second flexure mode gage SS02CC [leading edge root, concave side, 5.08 mm (0.20 in.) above the outsert] was the highest stressed location with SD06CC (leading edge lower

airfoil, concave side) being the second highest. Strain gage SD08CC (trailing edge lower airfoil, concave side) was maximum in the first torsional mode.

The data from the strain distribution testing also permitted experimentally defining the Campbell diagram for the rotor system. While set up with the air injection plate, the blade and trunnions vibratory characteristics were further explored and the Campbell diagram determined. This consisted of determining the points where the first three vibratory mode lines (1F, 2F and 1T) cross the various rotor excitation lines. The experimentally determined Campbell diagram is shown in Figure 23. This agrees closely with the predicted Campbell diagram and indicates an acceptable aeromechanical design.

Steady state centrifugal and bending stresses were also determined throughout the full speed range using the four steady-state gages. For these runs, no air excitation was used. The rotor speed was increased to a 100% load condition (3326 rpm) in increments of 20%. This loading corresponded to 105% of mechanical design load. These data are summarized in Table VII and plotted in Figure 24, as stress versus percent load. In order to compensate for strain gage output as a result of temperature effect, an apparent strain test was conducted on this blade prior to going into the whirligig. This involved heating the blade in an oven to 393 K (248° F) and recording the strain due to thermal expansion. These data were then factored into the whirligig steady-state strain readings. Blade temperatures were recorded simultaneously with strain gage readings. The data shows that the measured tensile stresses in the root region were 87 to 169 MN/m<sup>2</sup> (12.6 to 24.5 ksi) with the maximum measured stress appearing near the leading edge on the concave side, adjacent to the outsert. The stress measured in the airfoil leading edge region, concave side, slightly above the platform was 145 MN/m<sup>2</sup> (21 ksi). These stress levels are consistent with predictions and indicate an acceptable design.

Table VII. Steady State Stress Distribution Summary.

S/G No. % Load*	Steady State Stress, MN/m <sup>2</sup> (ksi)			
	SS01	SS02	SS03	SS04
40	46 (6.6)	67 (9.7)	12 (1.7)	63 (9.2)
60	61 (8.9)	106 (15.4)	14 (2.1)	91 (13.2)
80	74 (10.7)	141 (20.5)	17 (2.4)	119 (17.2)
100	87 (12.6)	169 (24.5)	17 (2.5)	145 (21.0)

\* Average of three runs

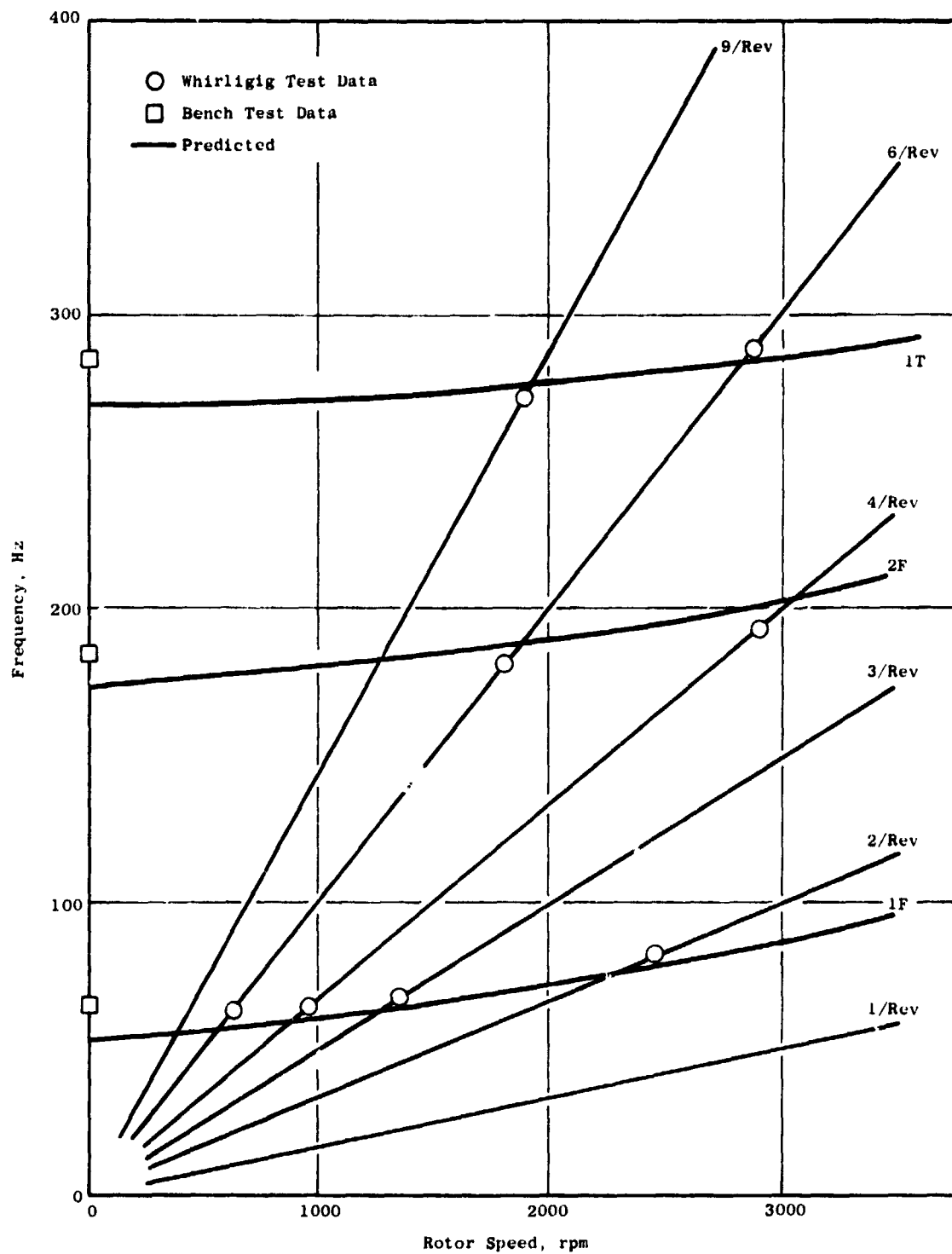


Figure 23. Experimentally Determined Campbell Diagram.

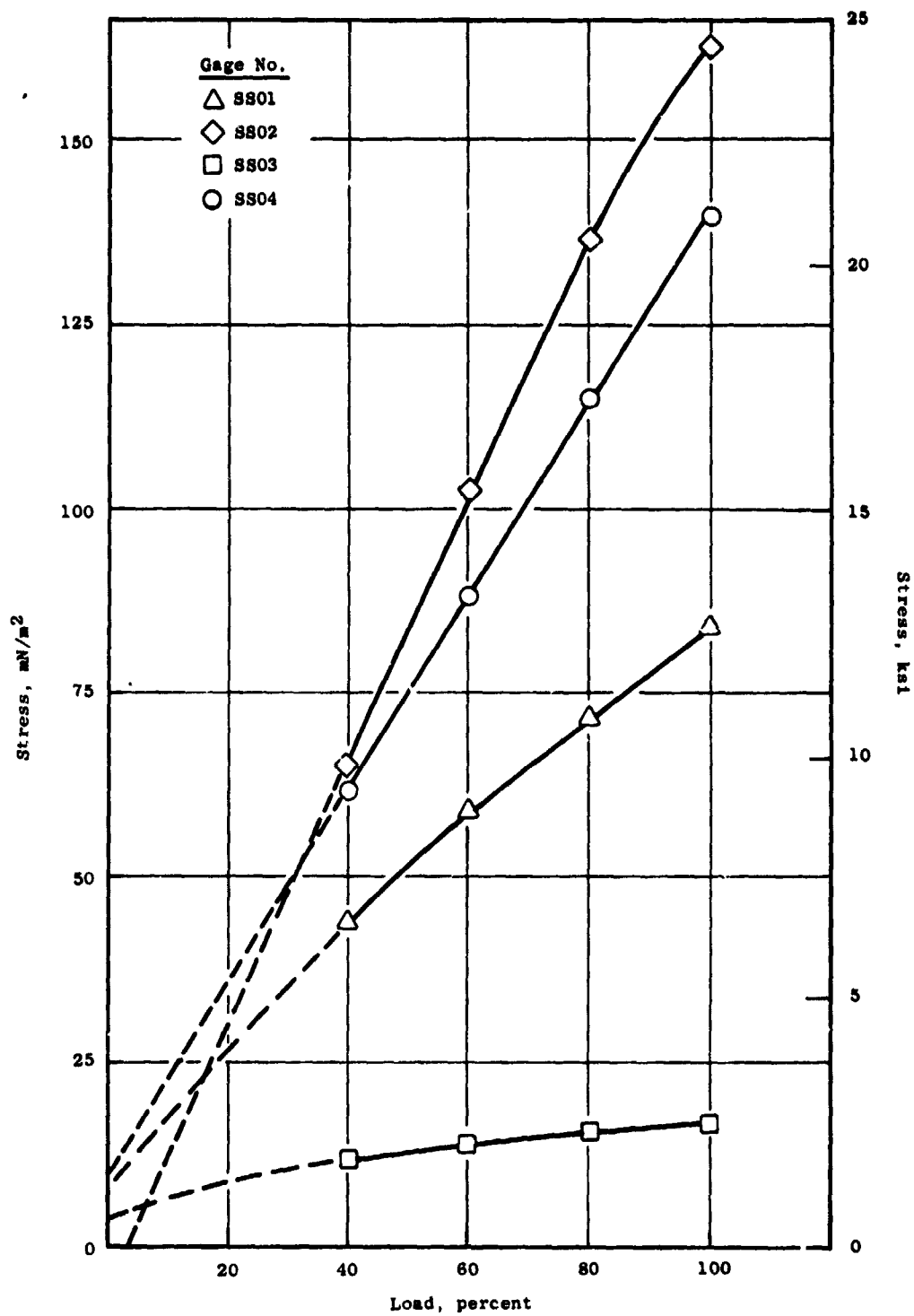


Figure 24. Steady-State Stress Distribution.

## 6.2 CYCLIC TESTING

Two blades, Q6 and Q7, were tested in low cycle fatigue (LCF) to determine the adequacy of the blades for this mode of loading. Each blade was tested in the whirligig for a total of 1000 cycles. Each cycle consisted of speedup to 3500 rpm (116% mechanical design load) and return to idle at 450 rpm. Temperatures were monitored to ensure that the blades were not overheated. The test on blade Q6 was interrupted every 100 cycles to conduct a dovetail inspection.

Blade Q7 was LCF tested following the completion of stress distribution testing. Blade Q6 was LCF tested following the completion of whirligig overspeed testing which is described in Section 6.3.

Posttest inspection of the blades consisted of ultrasonic C scanning, die penetrant examination and frequency measurement. Die penetrant inspection of blade Q7 showed signs of a crack in the trailing edge dovetail face. Ultrasonic inspection showed no signs of delamination and frequency measurement showed no loss in frequency. It was concluded that the blade was not structurally damaged. The ultrasonic, die penetrant and frequency inspection of blade Q6 showed no signs of damage and no loss in frequency. The moly-coated aluminum outsert of blade Q6 showed signs of wear and local loss of the molycoat along a chordwise line that coincides with the trunnion interface. This is shown in Figure 25.

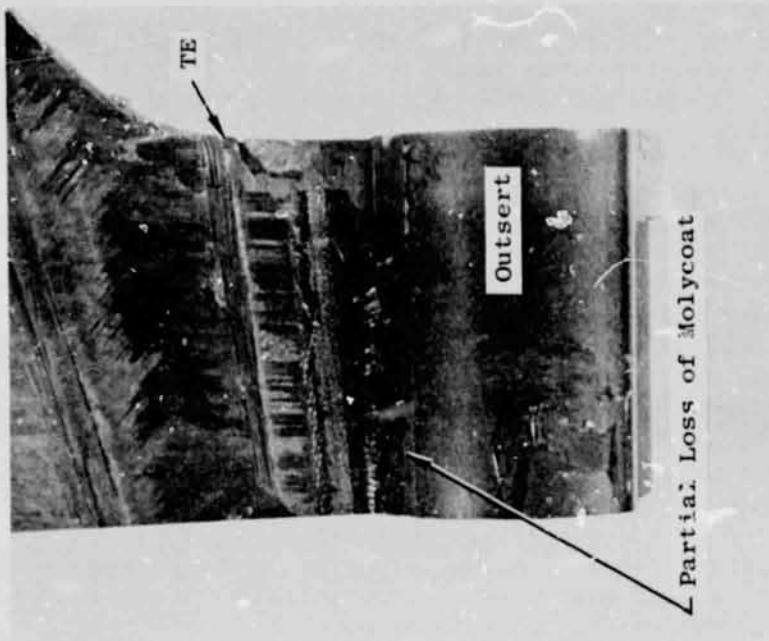
## 6.3 OVERSPEED PROOF TESTING

Blade Q6 was installed in the whirligig facility and was subjected to an overspeed test to evaluate the capability of the blade up to 117% mechanical design speed. The blade was instrumented with three thermocouples. This test was completed successfully with the blade being accelerated to 3800 rpm and held for 5-1/2 minutes. Posttest ultrasonic and die penetrant inspection revealed no blade damage.

## 6.4 HIGH CYCLE FATIGUE TESTING

Blade Q7 was high cycle fatigue tested in its first flexural mode in the whirligig facility to assess blade capability under vibratory loading combined with centrifugal steady-state loads. This test was conducted following the low cycle fatigue test. The high cycle fatigue testing was accomplished by holding the rotor speed constant at the point on a Campbell diagram where the excitation line crosses the desired mode line (see Figure 23). One strain gage at a high radial stress location (gage SD10CX of Figure 18) was used to establish the level of load excitation. The blade maximum stress was taken as the midchord convex location at a point slightly above the top of the platform as determined from bench tests on the final and preliminary blades. The other gages were monitored while the blade was being excited to fatigue or until the desired number of cycles had been reached. All gages

ORIGINAL PAGE IS  
OF POOR QUALITY



Concave Side

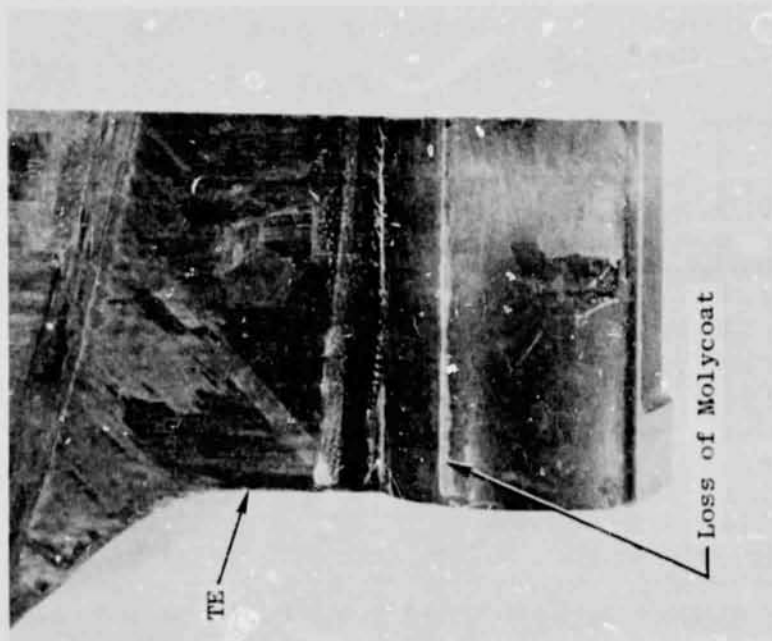


Figure 25. Blade Q6 Outsert After Overspeed and LCF Testing, Platform and LE Portion of Blade Root Removed.

were monitored during actual cycling in the event the strain gage being used for control should fail, then a gage at a lesser strain location would be used to establish the level of load excitation.

The blade was excited at a 2/rev crossover speed of 2320 rpm. The initial peak double amplitude stress was taken at  $122 \text{ MN/m}^2$  (17.7 ksi) at the maximum stress location. The maximum stress location was identified to be at the location of gage 10CX on strain distribution blade Q11 as discussed in Section 5.3. Strain gage number SD10 on blade Q7 was monitored for control at 46% of maximum blade stress as determined for this location in the bench strain distribution test. Blade radial elastic modulus was taken as  $10 \times 10^6$  psi as with the bench test blades. The blade successfully completed 3 million cycles with no loss in frequency. Double amplitude stress was increased to  $181 \text{ MN/m}^2$  (26.3 ksi) and the blade tested for another 3 million cycles, again with no loss in frequency. At a third level of  $253 \text{ MN/m}^2$  (36.7 ksi) the frequency dropped from 76.7 to 76 Hertz, after 3 million cycles. At  $347 \text{ MN/m}^2$  (50.3 ksi) the frequency dropped to 74 Hertz after 1.6 million cycles. These data are reported in Table VIII. Posttest die penetrant results are shown in Figure 26. The platform was removed from the blade to permit detailed ultrasonic inspection of the lower airfoil. This inspection showed the blade to be delaminated in the airfoil to root transition region. The molycoated aluminum outsert of blade Q7 showed signs of wear and some local loss of the molycoat along a chordwise line that coincides with the trunnion interface, somewhat less severe but similar to blade Q6.

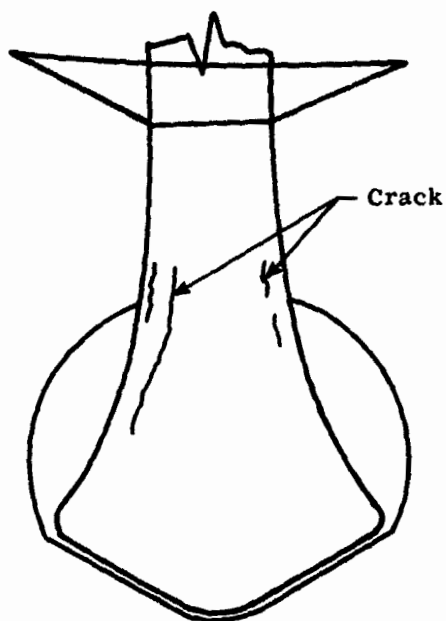
Table VIII. Whirligig First Flexural High Cycle Fatigue Test Summary, Blade Q7.

Double Amplitude Max. Stress $\text{MN/m}^2$ (ksi)	No. of Cycles $\times 10^6$	Speed rpm	Frequency Hertz	
			Start	End
122 (17.7)	3.0	2430/2320	76.7	76.7
181 (26.3)	3.0	2300	76.7	76.7
253 (36.7)	3.0	2320	76.7	76.0
347 (50.3)	1.6	2320	76.0	74.0

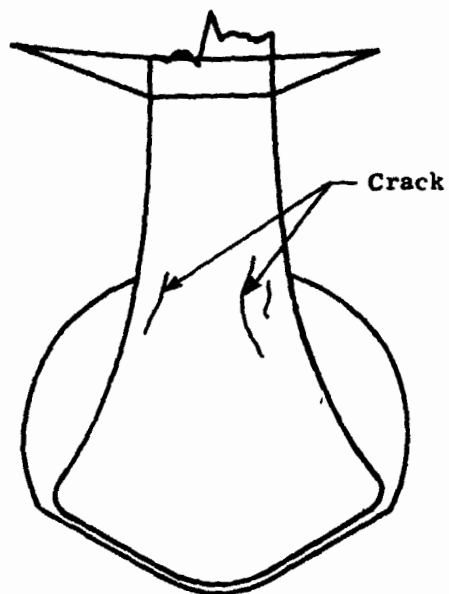
The results of this test and the bench high cycle fatigue tests were used to verify the stress range diagram for the blade, shown in Figure 27. This diagram is in agreement with the predicted stress range diagram shown in Reference 1. The region of the diagram enclosed by dotted lines was investigated by the testing in this program and will be used in establishing engine operating limits.



ORIGINAL PAGE IS  
OF POOR QUALITY



Trailing Edge



Leading Edge

Figure 26. Posttest Evaluation Blade S/N Q7.

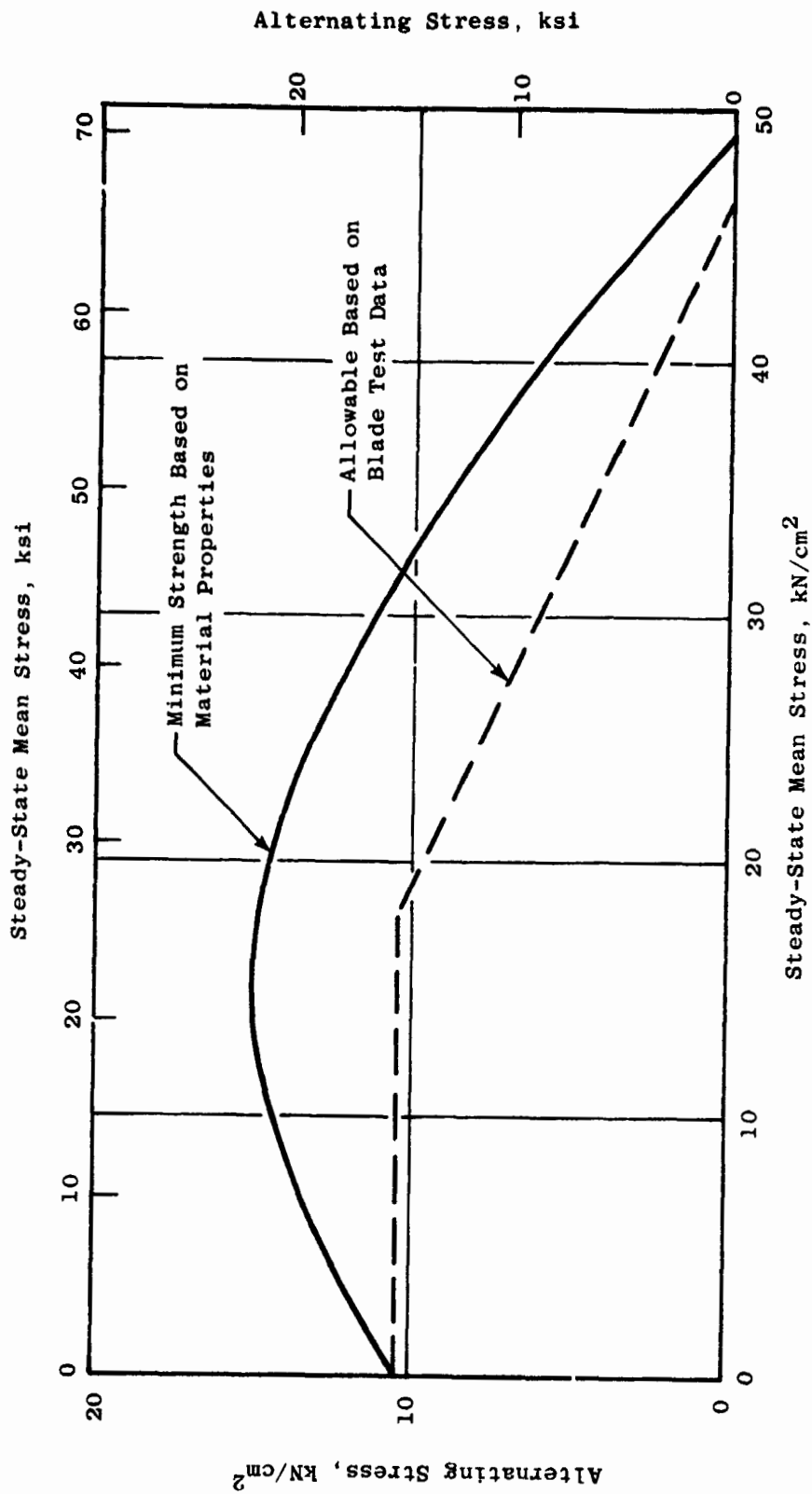


Figure 27. Allowable Stress Range Diagram - Blade Radial Stress.

These data, along with the design analysis, shows satisfactory margin for safe engine operation.

#### 6.5 BLADE PROOF TESTING

The 22 blades planned for use in the engine were individually proof spin tested in the whirling facility. Each blade was accelerated to 3400 rpm and held at this speed for 15 seconds. Posttest inspection was conducted and consisted of visual inspection and die penetrant examination of the blade dovetail faces and root undercut region. No damage was found. Table IX lists the serial numbers of the proof tested blades.

Table IX. Blades Whirling Proof Tested.

(15 seconds at 3400 rpm)

<u>S/N</u>	<u>S/N</u>
Q12	Q25
Q14	Q26
Q15	Q27
Q17	Q28
Q18	Q29
Q19	Q31
Q20	Q32
Q21	Q34
Q22	Q36
Q23	Q37
Q24	Q38

## 7.0 CONCLUSIONS

The completion of the QCSEE final design composite blade test program provides the following conclusions:

- Blade frequencies and mode shapes are close to predicted and are within the design tolerance.
- The final blade and platform design satisfies all aeroelastic and structural strength requirements of the program demonstrating suitability for engine operations.

## 8.0 REFERENCES

1. Advanced Engineering and Technology Programs Department - General Electric Company: Quiet Clean Short-Haul Experimental Engine (QCSEE) Under-the-Wing Engine Composite Fan Blade Design - NASA CR-134840, May, 1975.
2. Advanced Engineering and Technology Programs Department - General Electric Company: Quiet Clean Short-Haul Experimental Engine (QCSEE) Under-the-Wing Engine Composite Fan Blade Preliminary Design Test Report - NASA CR-134845, September, 1975.